1964

Gamma dosage in the vicinity of cylindrical voids in shields

Donald Stuart Sasscer
Iowa State University

GAMMA DOSAGE IN THE VICINITY OF CYLINDRICAL VOIDS IN SHIELDS

by

Donald Stuart Sasscer

A Dissertation Submitted to the
Graduate Faculty in Partial Fulfillment of
The Requirements for the Degree of
DOCTOR OF PHILOSOPHY

Major Subject: Nuclear Engineering

Approved:

Signature was redacted for privacy.
In Charge of Major Work

Signature was redacted for privacy.
Head of Major Department

Signature was redacted for privacy.
Dean of Graduate College

Iowa State University
Of Science and Technology
Ames, Iowa

1964

TABLE OF CONTENTS

INTRODUCTION

As the art of radiation shielding progresses toward the science of radiation shielding many new problems have been imposed upon the nuclear field. The overdesign philosophy sometimes used in the past, which was adequate when the shielding requirements were small or when weight or size were not a primary consideration, is no longer acceptable. The cost of shielding a large reactor facility is a significant portion of the total cost of the reactor and weight will undoubtably be a prime consideration for any shielding carried on space vehicles.

One of the problems requiring a more exact solution than has been available in the past is the prediction of the effect of voids or ducts in gamma shielding.

The purpose of this investigation was to determine the rate at which energy is absorbed in water at the surface of cylindrical ducts through an otherwise homogeneous shield which is assumed to be infinite in extent and 200 cm thick. The centerlines of the ducts were perpendicular to the direction of infinite extent and a one disintegration per second, isotropic, point source of cobalt 60 was located on the centerline and at mid-thickness.

The usually mathematical methods of solving gamma transport problems are based upon the Boltzmann transport equation. The steady state form of this equation is

$$\nabla \cdot \vec{\Omega}\, I(\vec{r}, \lambda, \vec{\Omega}) + \mu\, I(r, \lambda, \vec{\Omega}) = \int_0^{\lambda} \int_{4\pi} I(\vec{r}, \lambda', \vec{\Omega}')\, nk(\lambda', \lambda)\, \frac{\delta(1+\lambda'-\lambda-\vec{\Omega}\cdot\vec{\Omega}')}{2\pi}\, d\vec{\Omega}'\, d\lambda' + S(\vec{r}, \lambda, \vec{\Omega})$$

where

$I(\vec{r}, \lambda, \vec{\Omega})$ = the angular energy flux = the energy of photons of wave length λ in range $d\lambda$ and moving in the direction of the unit vector $\vec{\Omega}$ in the element of solid angle $d\vec{\Omega}$ which cross in unit time through a unit area located at the point $\vec{r}$ whose normal is in the direction $\vec{\Omega}$.

$\vec{r}$ = the position vector

= a unit vector in the direction of the photon velocity

λ = the wave length, in units of Compton wave length = $0.02426\ A^{\circ}$

μ = absorption coefficient

n = the number of nuclei per unit volume

$k(\lambda', \lambda)$ = the differential cross section for scattering from wave length λ' to wave length λ. From the Klein-Nishina formula, the function k in Thomson units per electron has the form

$$k(\lambda', \lambda) = \frac{3}{8}\frac{\lambda'}{\lambda}\left[\frac{\lambda}{\lambda'} + \frac{\lambda'}{\lambda} + 2(\lambda' - \lambda) + (\lambda' - \lambda)^2\right], \quad \lambda' < \lambda < \lambda' + 2$$

$$= 0 \text{ otherwise.}$$

$\frac{\delta(1 + \lambda' - \lambda - \vec{\Omega} \cdot \vec{\Omega}')}{2\pi}$ = the delta function relating the change in wave length to the change in angle for Compton scattering.

$S(\vec{r}, \lambda, \vec{\Omega})$ = the gamma source.

The Boltzmann equation cannot, in general, be solved rigorously. A large variety of methods exists for obtaining approximate solutions to this equation for special cases. However, the complicated form of the scattering kernel and the nonanalytic character of the absorption coefficient practically ensure that any accurate method of solving the transport equation be seminumerical in nature and involve extensive computation.

After consideration of various possible methods it was decided that the method of random sampling, i.e. the Monte Carlo method, would be the best approach to use in solving the problem undertaking in this investigation since it is the Monte Carlo technique that facilitates solving problems of complicated geometry.

REVIEW OF LITERATURE

The applicability of a few methods of solution of the Boltzmann equation for the rate at which energy is absorbed in the vicinity of shielding ducts is discussed below.

The "Straight-Ahead" Method

At high energies Compton scattering is mostly at small angles; even so, the photon loses, on the average, a large fraction of energy per collision. This observation inevitably suggested a treatment which neglects the angular deviation caused by a scattering collision but follows the energy degradation as closely as possible. One envisions the photon as continuing straight ahead in the direction in which it was emitted, but losing energy on each collision. A detailed discussion of this method is given by Foldy (1) and Bethe et al. (2). Wilkins (3) and Bethe (2) attempted to improve on the straight-ahead approach by using piecewise analytical fits to the μ-curve. Welton (4), Solon and Wilkins (5) and Solon, Wilkins et al. (6) also attempted to improve on the straight-ahead approach by using a root-mean-square angular spread.

These methods lead to improved answers for heavy materials but, as it turns out, the "rms" method is less accurate for light elements than the straight forward application of the straight-ahead method. (7). Due to the gross, and sometimes unknown, errors introduced by the straight-ahead method, this approach has fallen into disrepute and is seldom used.

Method of Successive Scattering

The method of successive scattering is the method of determining the flux of n-th scattered photons by using the collision density of the

(n-1) st scattered photons as the source.

The calculation of the uncollided flux is relatively simple. From the uncollided flux one can calculate the collision density for first scattering, and by treating such scattering collisions as a new source, the flux of singly-scattered photons can be found. In principle, the process can be repeated until all photons making significant contributions to the flux would be included. After the first scattering, however, the mathematics becomes quite involved. (8).

Considerable work has been done by Peebles on attenuation through an infinite plane slab for photons incident perpendicularly and obliquely to the slab. (9, 10, 11).

The method of successive scattering depends on a recursion relation between the transmission through a slab of the n-th collision photons and the (n-1)st collision photons. Unfortunately the recursion relation is such that only for slab geometries can the integrations be carried out successfully. Thus, this method is excluded as a means of attack on the problem at hand.

Method of Moments

The steps involved are similar to those in the "spherical-harmonic" method used in neutron slowing-down theory in which the angular flux is expanded in terms of Legendre polynomials. The resulting system of equations is usually solved by numerical methods to obtain the coefficients so that the expansion approximates the solution of the Boltzmann equation. The more the number of terms in the expansion, the greater will be the accuracy of the resulting solution. (12, 13, 14).

The most serious restriction of this method is that, regardless of the number of terms in the expansion, the moment method is restricted to infinite media. (7) In obtaining the solution an integration by parts is performed, in which the integrated terms vanish only if the integration is over all space. Thus in the region near a boundary, as exists in the problem under investigation, the moment method breaks down.

Laplace Transform Method (Asymptotic Solutions)

Considerable effort has been devoted by Wick (15), Fano (16) and Spencer (17) to finding the general behavior of the flux for very deep penetrations. The asymptotic methods involve working with the spatial Laplace transform of the angular flux I rather than with I itself. The nature of the solution of the Boltzmann equation is such that the inverse transform integral can be most easily evaluated for large x. Indeed solutions are difficult for distances less than 10 mean free paths, however, unlike the moment method, the labor does not increase with distance of penetration and the spectrum at 100 mfp can be quite easily obtained. This method is obviously not suited for the problem at hand.

Gamma Albedo Method

The radiation scattered from thick surfaces consists largely of multiple-scattered radiation. For this reason single-scattering theory is inadequate in surface-scattering problems, and the albedo theory must be employed. Gamma albedo is the ratio of emergent to incident gamma ray energy.

The Naval Research Laboratory (18) has obtained the albedo for iron and water at several incident angles and Rockwell (19) has interpolated

the NRL data and presented gamma albedo for photons at any incident angle as a function of the emergent angle.

The gamma albedo method holds considerable promise for determining the flux in many types of shielding voids. Price (20), in drawing some general conclusions concerning streaming in ducts, discusses first the case of a duct filled with a material much less dense than the shield and then goes on to say

> Secondly, owing to the low albedo for gamma radiation ...caution should be used in oversimplifying the analysis for points outside the duct; in general a ray analysis ... does not reproduce at all satisfactorily the observed gamma-ray intensities in the vicinity of a duct.

The Method of Random Sampling (Monte Carlo)

The Monte Carlo technique might be described as a theoretical experiment in which a large number of photons are released from the source and their subsequent life histories traced until all of the photons are enventually absorbed. This method consists of replacing the actual physical experiment by an analogous numerical process that enables one to predict the data that would be obtained by the physical experiment. Each step used in obtaining the history of a photon is chosen at random out of the known probability distribution for the given event--absorption, collision, etc. The random choice might very well be made by the throw of dice or spin or a roulette wheel but is in practice determined from a sequence of random numbers.

Kahn (21, 22] presents a good introduction of the use of the Monte Carlo process for gamma shielding. Welton (4) discusses the accuracy of Monte Carlo calculations and Goldstein (7) reviews some of the uses that

have been made of the Monte Carlo technique in gamma shielding. Collins (23) has applied the Monte Carlo technique to streaming in ducts and has obtained data that differ from experimental data by a maximum of less than 10 percent.

The outstanding features of the Monte Carlo method are its great flexibility and adaptability to complex boundary conditions on one hand, and the laboriousness of the calculations required by this method on the other. Fano (14) analyzes the type of problem best suited to an attack by Monte Carlo when he says

> The indicated features suggest the possibility of separating boundary problems into two parts: (1) The penetration of the radiation from the source to the vicinity of a boundary, and (2) the effect of the boundary. One can often solve problem (1) for an infinite homogeneous medium by the various methods described in parts B and C of this article and then superimpose a solution of problem (2) obtained by random sampling. Thereby one takes advantage both of the efficiency of the analytical method and of the flexibility of the Monte Carlo method.*

---

*Parts B and C of Fano's article describe the method of moments, the successive scattering technique and various asymptotic solutions.

NOMENCLATURE AND GEOMETRY

In order to simplify the program, and thereby save computer time, several approximations to the physical conditions were made.

a. A void exists inside the ducts.

b. The source is a point source.

c. A water shield of 60 cm in extent will have the same rate of energy absorbed at the surface of the duct as a water shield of infinite extent.

Since the density of air is only slightly greater than 0.1 percent of the density of water and since the absorption coefficients in cm^2/gm are approximately equal, no appreciable error is introduced by assuming the ducts consist of a void instead of air.

A point source never exists in nature. However, since actual sources exist in various sizes and shapes, it was thought best to base this investigation on the idealized case of a point source.

A distance of 60 cm in water represents approximately 4 mfp for unscattered cobalt-60 photons. Thus, in order for a photon to have a scattering collision at a distance greater than 60 cm from the void and still contribute to the rate at which energy is absorbed at the surface of the void, the photon would have to travel a distance greater than 4 mfp radially, then backscatter another 4 mfp. This results in the photon having a probability of less than e raised to the negative eighth power of contributing to the rate at which energy is absorbed at the surface. Therefore the error introduced by assuming that the shield is only 60 cm in extent, which means that no photon can undergo a scattering collision

at a distance greater than 60 cm from the surface, would be negligible.

Since the shield and duct are symmetrical about the mid-thickness, data are obtained over only a half-thickness of the shield.

The state of the gamma ray just before the n-th collision is characterized by 5 quantities illustrated in Figure 1 where

x_n = position along centerline = the component of the distance from the source to location of the n-th collision in the direction of the centerlime of the duct.

r_n = position along radius = the component of the distance from the source to location of the n-th collision in the direction perpendicular to the centerline of the duct.

λ_n = wave length of photon in Compton units.

$\vartheta_n = \cos^{-1} (\vec{\omega}_n \cdot \vec{j})$ where $\vec{j}$ is a unit vector in the direction of the duct centerline.

$\phi'_n = \cos^{-1} \left(\frac{\vec{\omega}_n \cdot \vec{i}_n}{\sin \vartheta_n}\right)$ where $\vec{i}_n$ is a unit vector in the direction perpendicular to the duct centerline.

The vectors

$$\vec{r}_n = (r_n, x_n)$$

and $\vec{\omega}_n = (\sin \vartheta_n \cos \phi'_n, \sin \vartheta_n \sin \phi'_n, \cos \vartheta_n)$

indicating the position and direction of the photon are also shown in Figure 1.

Figure 1. Geometry

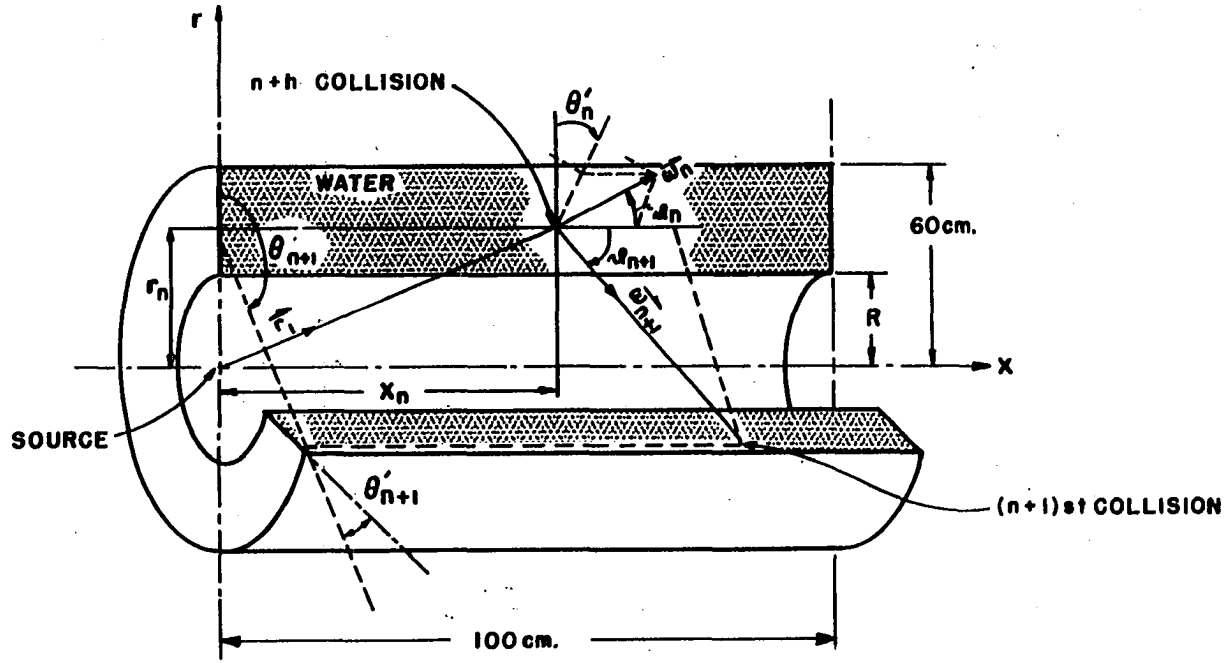
r
n+h COLLISION
θ'_n
WATER
60cm.
θ'_{n+1}
r_n
R
X
x_n
SOURCE
θ'_{n+1}
(n+1)st COLLISION
100 cm.

THE PROGRAM

Main Program

The flow sheet describing the main program is given in Figure 2. The steps in the program are as follows:

1. The wave length, λ_1, position, x and r, and the azimuthal angle, ϕ_1', of the source photons are the same for all photons. The position of the first collision, x_1 and r_1, is determined by a programmed sequence of positions at which initial collisions are allowed to occur. Then the angle between the direction of the source photon and the duct centerline, ϑ_1, and the first collision weight factor, W_1, are calculated.

2. A test comparing the scattering cross section at λ_n to the total cross section at λ_n is made to determine whether the photon undergoes a scattering or an absorbing collision. If an absorbing collision occurs (i.e. the photon does not "survive" the collision) the energy of the photon is deposited at the location of the collision by the ENERGY ABSORBED subroutine and the program starts over again with a new photon. If a scattering collision occurs the program proceeds to the CHANGE IN WAVE LENGTH subroutine.

3. The change in wave length is calculated by the Klein-Nishina formula and the energy loss by the photon is recorded by the ENERGY ABSORBED subroutine. If $\lambda_n > 10.22$ Compton units the history is ended after the energy loss has been recorded. If $\lambda_n < 10.22$ Compton units, the change in direction is calculated after the recording of the energy loss.

Figure 2. Flow diagram of main program

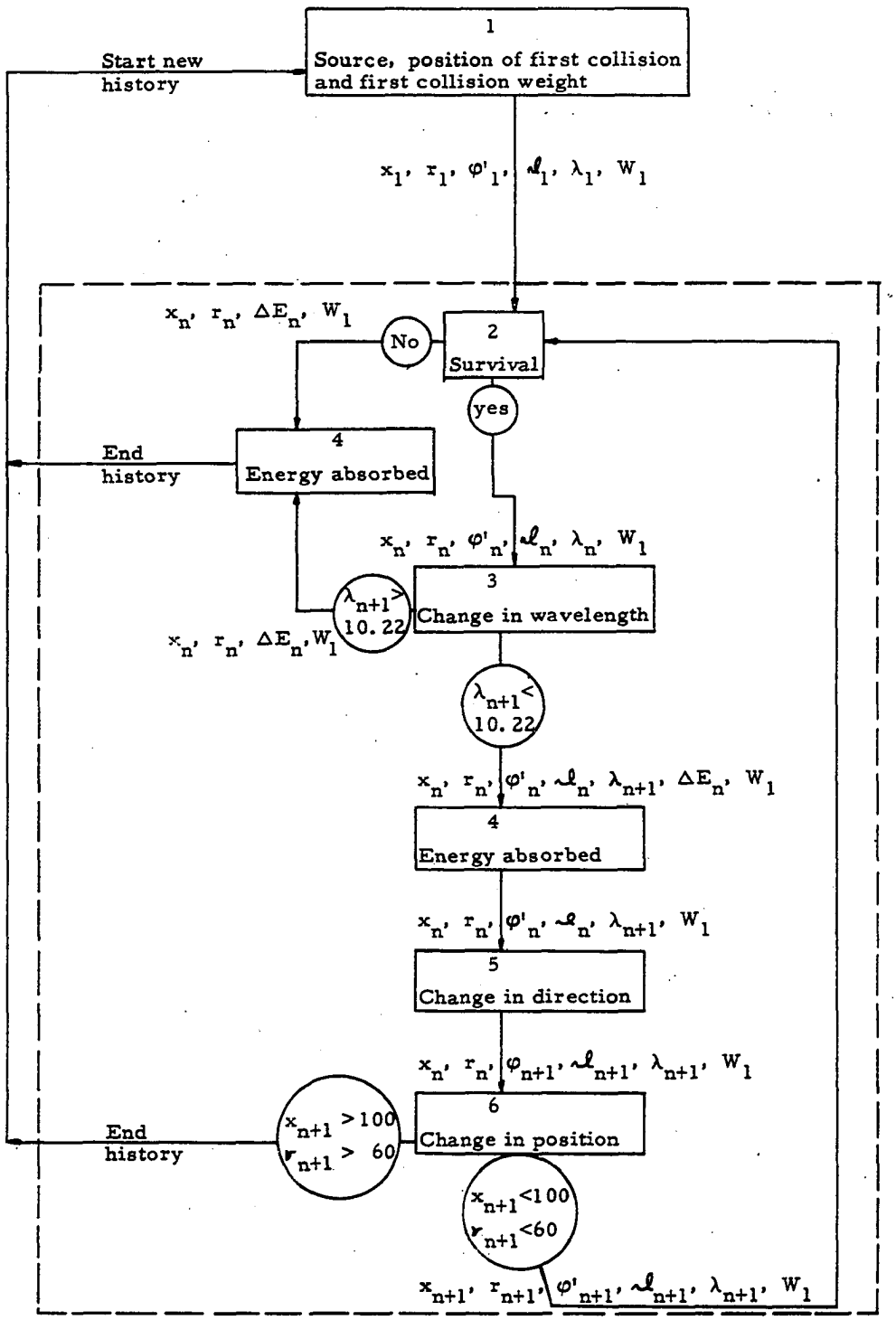
1
Source, position of first collision and first collision weight
Start new history
x_1, r_1, φ'_1, μ_1, λ_1, W_1
x_n, r_n, ΔE_n, W_1
No
2
Survival
yes
4
Energy absorbed
End history
x_n, r_n, φ'_n, μ_n, λ_n, W_1
3
Change in wavelength
$\lambda_{n+1} > 10.22$
x_n, r_n, ΔE_n, W_1
$\lambda_{n+1} < 10.22$
x_n, r_n, φ'_n, μ_n, λ_{n+1}, ΔE_n, W_1
4
Energy absorbed
x_n, r_n, φ'_n, μ_n, λ_{n+1}, W_1
5
Change in direction
x_n, r_n, φ_{n+1}, μ_{n+1}, λ_{n+1}, W_1
6
Change in position
$x_{n+1} > 100$
$r_{n+1} > 60$
End history
$x_{n+1} < 100$
$r_{n+1} < 60$
x_{n+1}, r_{n+1}, φ'_{n+1}, μ_{n+1}, λ_{n+1}, W_1

4. The ENERGY ABSORBED subroutine is used to calculate the energy absorbed per unit volume and to record the amount of energy absorbed and the position at which the energy absorption occurs.

5. By using the Compton scattering formula, the change in direction of the photon is calculated from the change in wave length.

6. The position of the (n+1) st collision is determined from the position, direction and wave length of the n-th collision.

The program then tests for survival of the photon on the (n+1) st collision etc. Steps 2 through 6, enclosed by a dotted line in Figure 2, form the so called "loop" of the program. That is, the program proceeds through the steps (or subroutines) 2 through 6 and then back to 2 until the history of a photon is completed. After the history of one photon has ended the history of another photon is begun, starting with step 1. This process continues until the desired number of photon histories are acquired.

The program then adds the energy absorbed per unit volume in each of the volumetric rings of shielding material and divides the sum by the total number of photons used by the program, thus normalizing the results to a source of one disintegration per second. The final step in the program is the printing of the normalized rate of energy absorbed in Mev/cm^3-sec as a function of position.

A detailed description of the six subroutines is given in the following section.

Source, Position of First Collision and First Collision Weight

Source

Cobalt-60 emits two gamma rays per disintegration, one at 1.33 Mev and the other at 1.17 Mev. Goldstein (7) has analyzed the error in the rate at which energy is absorbed in gamma shields caused by assuming that cobalt-60 emits two photons of 1.25 Mev rather than a 1.33 Mev and a 1.17 Mev photon, and has found the error to be completely negligible. Therefore in this program a source of two 1.25 Mev gamma rays per disintegration and one disintegration per second was assumed.

Due to symmetry about $x = o$ it was assumed that each half-thickness of shield received one photon per disintegration. Since the source is at $r = o$ (Figure 1) the photons are emitted symmetrically with respect to ϕ, therefore ϕ_1 need not be specified.

Position of first collision

It was observed in test runs that those photons whose initial collisions were between 25 cm and 30 cm from the void contributed only approximately 1 percent to the rate at which energy was absorbed at the interface. For this reason, no initial collisions were assumed to occur at a distance greater than 27.5 cm from the void.

Figure 3 gives the cross section of one-fourth of the cylindrical shield showing the positions of the initial collisions, and the cross sections of the volumetric rings in which the initial collisions occur. It is assumed that all initial collisions in a volumetric ring occur along a circle (represented by a point in Figure 3) in the center of the ring.

Figure 3. Cross section of one fourth of shield

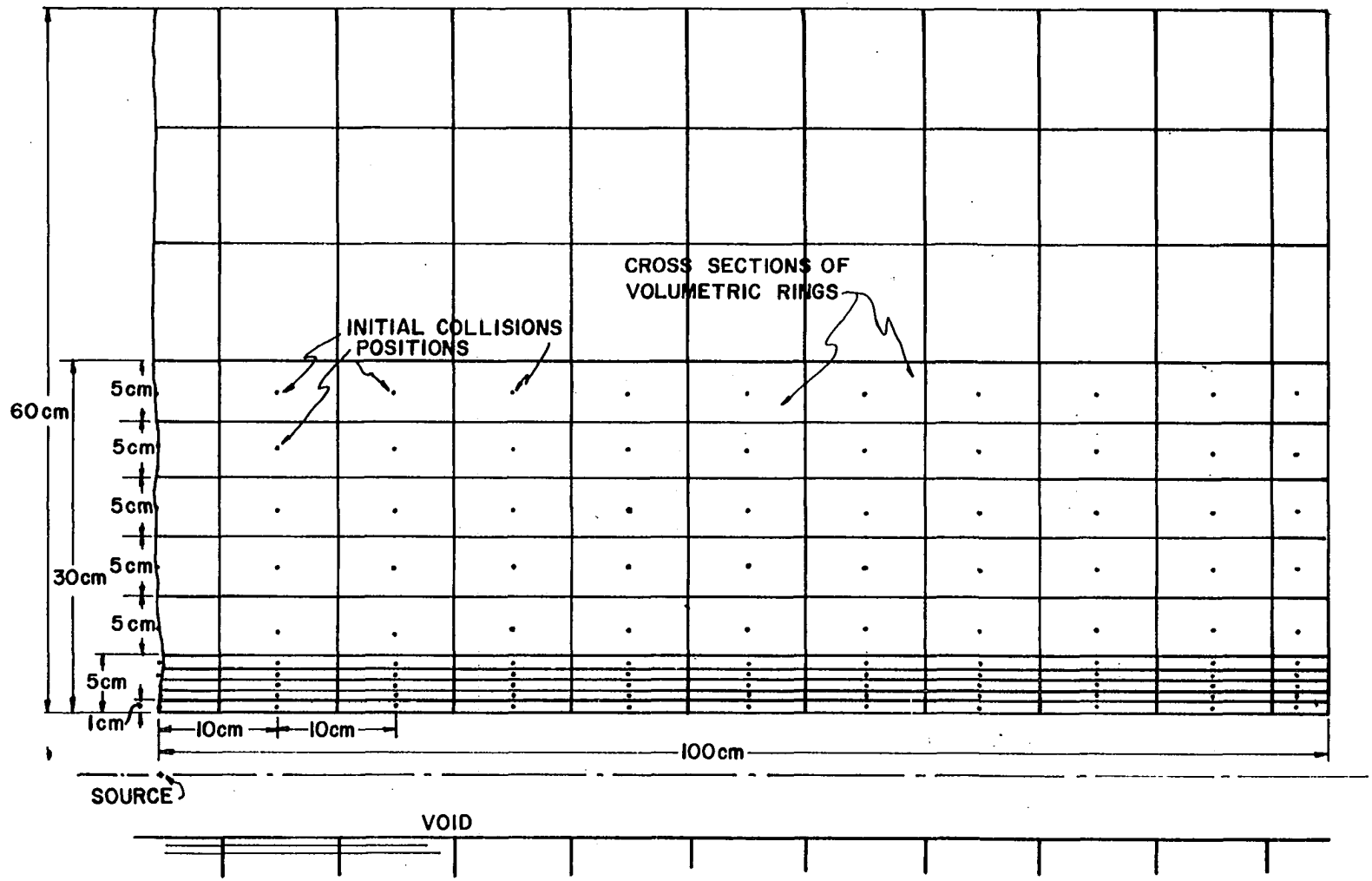
CROSS SECTIONS OF
VOLUMETRIC RINGS
INITIAL COLLISIONS
POSITIONS
60cm
30cm
5cm
5cm
5cm
5cm
5cm
5cm
1cm
10cm
10cm
100cm
SOURCE
VOID

Ducts with radii of 5 different sizes were investigated. R_i, i=1, 2, ... 5, representing the radius of a duct, is given by

$R_1 = 0$

$R_2 = 1$ cm

$R_3 = 2$ cm

$R_4 = 3.81$ cm

$R_5 = 10$ cm

The initial collisions occurred at radial distances of 0.5, 1.5, 2.5, 3.5, 4.5, 7.5, 12.5, 17.5, 22.5 and 27.5 cm from the interface. That is to say, the radius of the j-th circle, at which initial collisions occurred, in the shield having a duct of radius R_i is given by $(R_1)_i^j$ where

$$(r_1)_i^j = (r_1)_i^{j-1} + (\Delta r_1)^j \qquad j = 2, 3 \ldots 10$$

$$(r_1)_i^1 = R_i + 0.5 \text{ cm}$$

$$(\Delta r_1)^j = 1.0 \text{ cm} \qquad 2 \leq j \leq 5$$

$$(\Delta r_1)^6 = 3.0 \text{ cm}$$

$$(\Delta r_1)^j = 5.0 \text{ cm} \qquad 7 \leq j \leq 10$$

The initial collisions occurred at the x positions of 0, 10, 20 ... 90 and 97.5 cm. That is to say, the distance from the source, parallel to the duct centerline, to the k-th position at which initial collisions occurred is given by ${}_k(x_1)$

where

$${}_k(x_1) = {}_{k-1}(x_1) + {}_k(\Delta x)_k \quad = 2, 3 \ldots 11$$

$${}_1(x_1) = 0$$

$${}_k(\Delta x) = 10 \text{ cm} \qquad 2 \leq k \leq 10$$

$_{11}(\Delta x) = 7.5$ cm

First collision weight

Since the positions of the initial collisions are programmed to have a uniform density in the x-direction, it is necessary to correct the energy deposited by each scattering or absorbing collision by a weight factor. The weight factor of a photon that has its initial collision in the j-th ring and at the k-th position in the x-direction of the shield that has a duct of radius R_i is given by $_k(W_1)_i^j$. The weight factor is equal to the probability that the photon would have an initial collision in the volumetric ring at $_k(x_1)$ and $(r_1)_i^j$.

The weight factor (Appendix A) is given by

$$_k(W_1)_i^j = {}_k(P_{\vartheta_1})_i^j \; {}_k(P_{(\xi_1)_m})_i^j \; {}_k(V_1)_i^j \; (P_{v_1})_i \; (N_1)_i$$

where

$$_k(P_{\vartheta_1})_i^j = \text{area attenuation factor} = \frac{1}{4\pi \left([_k(x_1)]^2+[(r_1)_i^j]^2\right)}$$

$$_k(P_{(\xi_1)_m})_i^j = \text{material attenuation factor} = \mu_1 e^{-\frac{\mu_1((r_1)_i^j - R_i)([_k(x_1)]^2 + [(r_1)_i^j]^2)^{\frac{1}{2}}}{(r_1)_i^j}}$$

$$_k(V_1)_i^j = \text{volume factor} = \pi \left[(r_1)_i^j + \frac{(\Delta r_1)_j}{2})^2 - ((r_1)_i^j - \frac{(\Delta r_1)_j}{2})^2\right] (\Delta x_v)_k$$

where $(\Delta x_v)_o = 5$ cm

$(\Delta x_v)_k = 10$ cm $\qquad 1 \leq k \leq 9$

$(\Delta x_v)_{10} = 5$ cm

$$(P_{v_1})_i = \text{void factor}$$

$$= \cos\left(\tan^{-1}\frac{R_i}{100}\right)$$

$$(N_1)_i = \text{normalizing factor}$$

$$= \frac{1}{\sum_{k=0}^{11}\sum_{j=0}^{10} {}_k(P_{\nu_1})_i^j \; {}_k(P_{(\xi_1)_m})_i^j \; {}_k(V_1)_i^j \; (P_{v_1})_i}$$

Survival

A collision results either in absorption or scattering. If $\mu_{sc}(\lambda_n)$ is the probability, per centimeter of path length, of a photon of wave length λ_n undergoing a scattering collision in the shield, and if $\mu(\lambda_n)$ is the probability, per centimeter of path length, of a photon of wave length λ_n undergoing either an absorbing or scattering collision in the shield, then $\frac{\mu_{sc}(\lambda_n)}{\mu(\lambda_n)}$ equals the probability that a collision of a photon of wave length λ_n will be a scattering collision. Consequently $1 - \frac{\mu_{sc}(\lambda_n)}{\mu(\lambda_n)}$ equals the probability that a collision of a photon of wave length λ_n will be an absorbing collision. With the probability $1 - \frac{\mu_{sc}(\lambda_n)}{\mu(\lambda_n)}$, therefore, the n-th collision is allowed to result in absorption and the history is terminated. With the probability $\frac{\mu_{sc}(\lambda_n)}{\mu(\lambda_n)}$ the n-th collision is allowed to result in scattering and the history is continued.

Figure 4 gives the flow diagram for survival. Values for the ratio of the Compton scattering cross section $\mu_{sc}(\lambda_n)$ to total cross section $\mu(\lambda_n)$ (both without coherent scattering) as a function of energy were obtained from Grodstein (25). Grodstein's data were plotted and values of $\frac{\mu_{sc}(\lambda_n)}{\mu(\lambda_n)}$ for various intervals of energy were chosen so that the ratio at the midpoint of the interval was in all cases within 1 percent of the ratio at the extremes.

Figure 4. Flow diagram of survival subroutine

Input parameters = λ_{n+1}, $\frac{\mu_{sc}}{\mu_t}$

Output parameters = INDIC = 1 Photon scattered on n-th collision

INDIC = 0 Photon absorbed on n-th collision

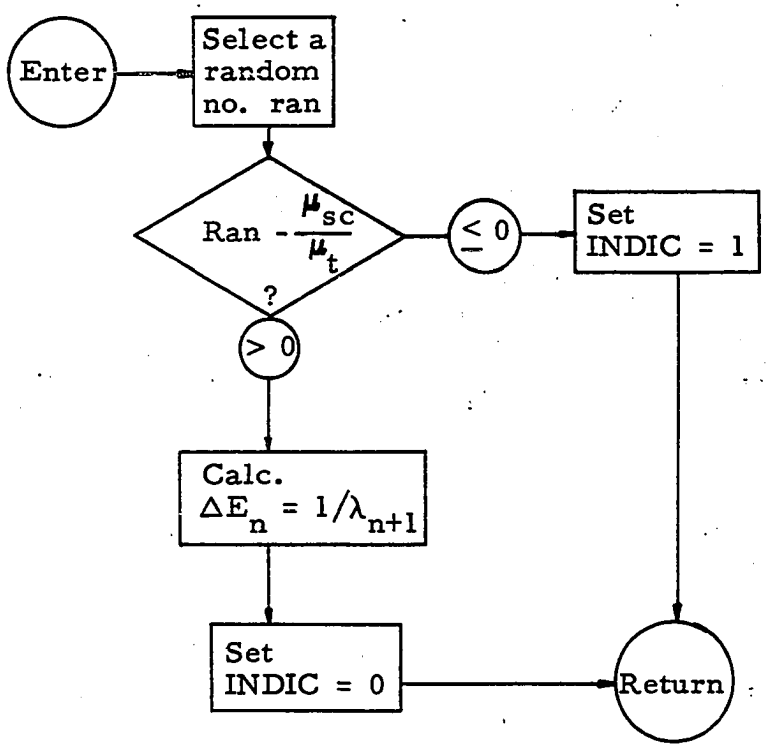

Change in Wave Length

The change in wave length was determined by the Klein-Nishina formula which takes on its simplest form if the wave length is expressed in units of the Compton wave length. The relation between λ in Compton units and E in Mev is given by

$$\lambda = \frac{0.5110}{E}$$

As mentioned in the INTRODUCTION, the Klein-Nishina formula is given by

$$k(\lambda_{n+1},\lambda_n) = \frac{3}{8}\frac{\lambda_n}{\lambda_{n+1}}\left[\frac{\lambda_{n+1}}{\lambda_n} + \frac{\lambda_n}{\lambda_{n+1}} + 2\ (\lambda_n-\lambda_{n+1})+(\lambda_n-\lambda_{n+1})^2\ \right],$$

$$\lambda_n \leq \lambda_{n+1} \leq \lambda_n + 2$$

$$= 0 \text{ otherwise.}$$

The method used to determine the change in wave length was suggested by Fano (14). This method combines the technique of obtaining random variates indirectly through the selection of a random number and of the rejection technique. Omitting the irrelevant normalization constant, one can express the Klein-Nishina distribution in the form

$$k\ (r,\ \lambda_n) = \frac{\lambda_n+2}{9\lambda_n+2}\ g_1(r)\ h_1(r) + \frac{8\lambda_n}{9\lambda_n+2}\ g_2\ (r)\ h_2(r)$$

where

$$r = \frac{\lambda_{n+1}}{\lambda_n}$$

$$g_1 = \frac{\lambda_n}{2} \qquad h_1 = 4\ \left(\frac{1}{r} - \frac{1}{r^2}\right)$$

$$g_2 = \frac{\lambda_n+2}{2r^2} \qquad h_2 = \tfrac{1}{2}\ \left[(1-\lambda_n r + \lambda_n)^2 + \frac{1}{r}\ \right]$$

To select a random variate from the distribution $k(r, \lambda_n)$ one first selects the random variate r with relative frequency $\frac{\lambda_n+2}{9\lambda_n+2}$ and $\frac{8\lambda_n}{9\lambda_n+2}$ from the related distribution functions $g_1(r)$ and $g_2(r)$ by the "cumulative probability" or "change in variable" method. Then one decides by the rejection technique, using $h_1(r)$ and $h_2(r)$, whether or not to accept r as a random variate of $k(r, \lambda_n)$. A flow chart of the sampling procedure is given in Figure 5. It can be shown (14) that the average number of random number triplets required to select a random variate r is less than 1.7 for all λ in the range investigated.

Energy Absorbed

Figure 6 gives the flow diagram for the energy that is absorbed. The volumetric rings in which the energy is absorbed are shown in Figure 3.

The radial distances from the centerline of the duct to the centers of the rings are 0.5, 1.5, 2.5, 3.5, 4.5, 7.5, 12.5, 17.5, 22.5, and 27.5 cm. That is to say, the radial distance to the center of the ℓ-th ring, in which energy is absorbed on the n-th collision in the shield having a duct of radius R_i, is given by $(r_n)_i^{\ell}$ where

$$(r_n)_i^{\ell} = (r_n)_i^{\ell-1} + (\Delta r_n)^{\ell} \qquad \ell = 2, 3 \ldots 10$$

$$(r_n)_i^{1} = R_i + 0.5 \text{ cm}$$

$$(\Delta r_n)^{\ell} = 1.0 \text{ cm} \qquad 2 \le \ell \le 5$$

$$(\Delta r_n)^{6} = 3.0 \text{ cm}$$

$$(\Delta r_n)^{\ell} = 5.0 \text{ cm} \qquad 7 \le \ell \le 10$$

Figure 5. Flow diagram of change in wave length subroutine

Input parameter = λ_n

Output parameters = λ_{n+1}, $\Delta\lambda_n$, ΔE_n, INDICW

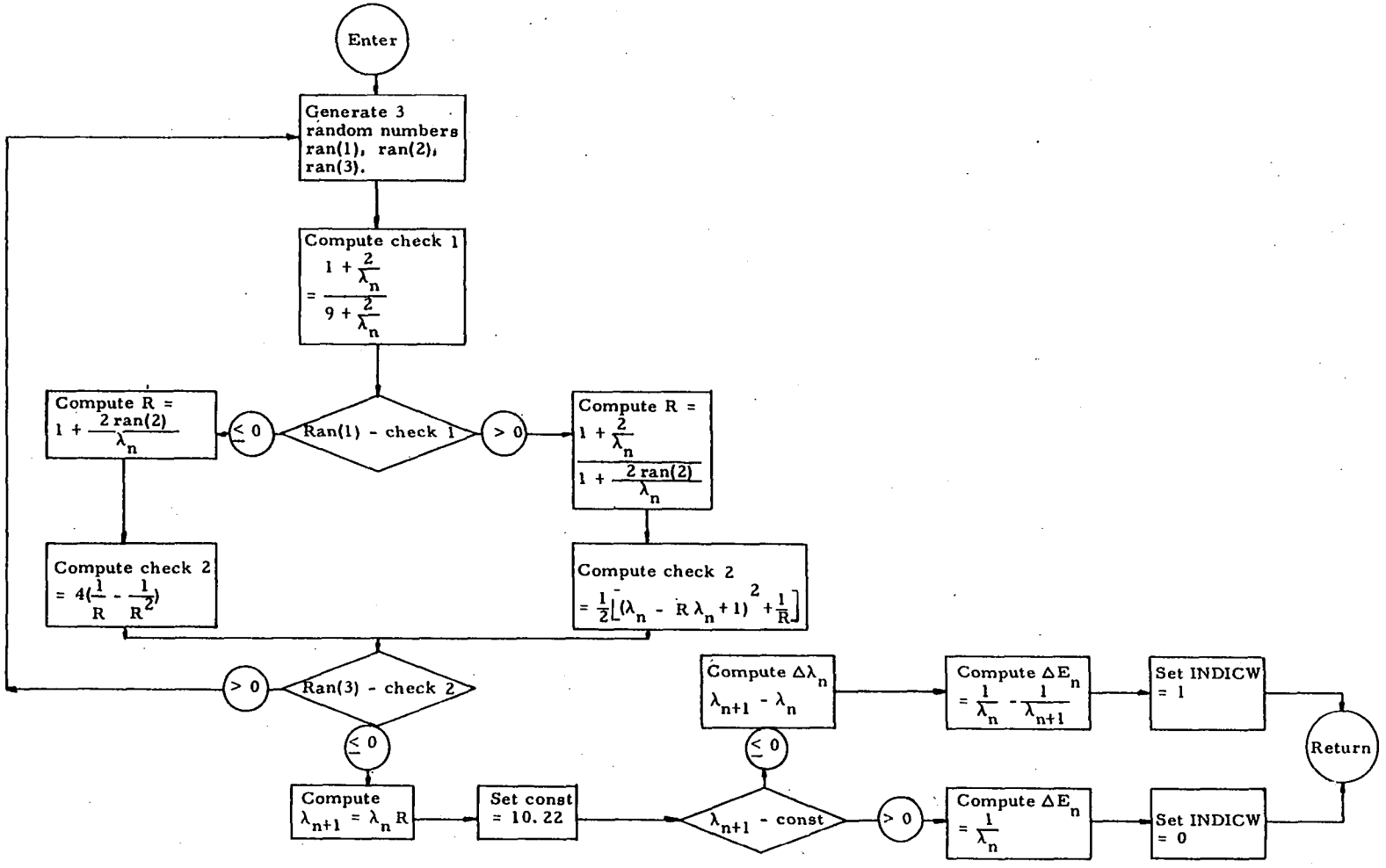

Figure 6. Flow diagram of energy absorbed subroutine

Input parameters = r_n, x_n, ΔE_n, W_1

Output = accumulated energy in energy matrix (E mat)

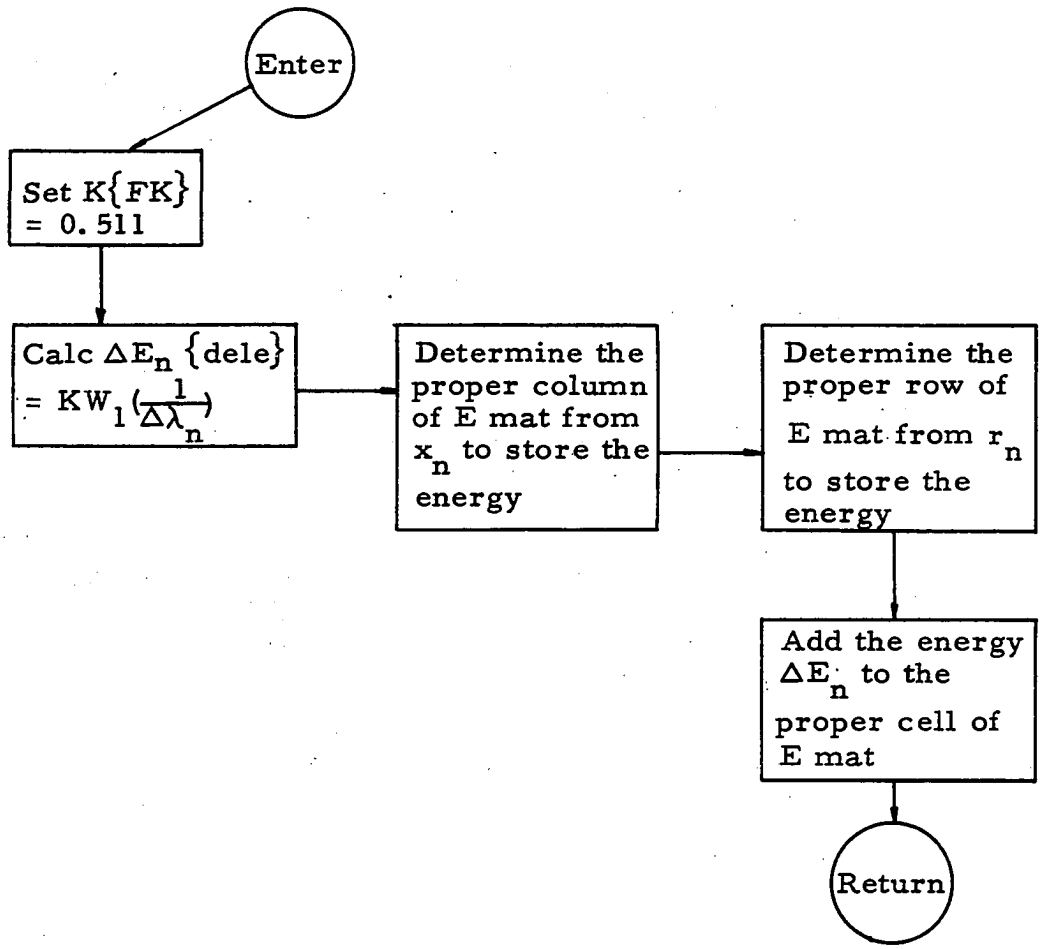

All of the rings have a width (in the x-direction) of 10 cm except the ring whose center is at x = o and the ring whose center is at x = 97.5 cm in which cases the widths are 5 cm. The m-th width, in the x-direction, of the volumetric ring, in which energy is absorbed in the n-th collision, is given by ${}_m(\Delta x_n)$ where

$${}_1(\Delta x_n) = 5 \text{ cm}$$

$${}_m(\Delta x_n) = 10 \text{ cm} \qquad 2 \leq m \leq 10$$

$${}_{11}(\Delta x_n) = 5 \text{ cm}$$

Thus the volume of the ℓ-th ring, which has the width ${}_m(\Delta r_n)$ in the x-direction, in which energy is absorbed on the n-th collision in the shield having a duct of radius R_i, is given by ${}_m(V_n)_i^{\ell}$ where

$${}_m(V_n)_i^{\ell} = \pi \left\{ \left[(r_n)_i^{\ell} + \frac{(\Delta r_n)^{\ell}}{2} \right]^2 - \left[(r_n)_i^{\ell} - \frac{(\Delta r_n)^{\ell}}{2} \right]^2 \right\}$$

Energy can be absorbed in ${}_m(V_n)_i^{\ell}$ by one of three methods:

1. by absorption of the photon on the n-th collision in which case the energy that is absorbed is equal to the energy of the photon times the weight factor of the photon. That is

$${}_m(\Delta E_n)_i^{\ell} = 0.5110 \; {}_k(W_1)_i^j \left(\frac{1}{\lambda_n}\right)$$

where ${}_k(W_1)_i^j$ is the weight factor of the photon which undergoes its initial collision in the j-th ring and at the k-th position in the x-direction of the shield that has a duct of radius R_i.

2. by scattering on the n-th collision when $\lambda_{n+1} < 10.22$ Compton units (i.e. $E_{n+1} > 0.050$ Mev) in which case the energy that is absorbed

is equal to the energy of the photon before the n-th collision less the energy of the photon after the n-th collision times the weight factor of the photon. That is

$$_m(\Delta E_n)_i^j = 0.5110 \; _k(W_1)_i^j \left(\frac{1}{\lambda_n} - \frac{1}{\lambda_{n+1}}\right)$$

3. by scattering on the n-th collision when $\lambda_{n+1} > 10.22$ Compton units, in which case the photon is assumed to be absorbed and

$$_m(\Delta E_n)_i^j = 0.5110 \; _k(W_1)_i^j \left(\frac{1}{\lambda_n}\right) \quad .$$

There are several reasons why a photon which has a wave length greater than 10.22 Compton units (i.e. $E_{n+1} < 0.050$ Mev) after collision is assumed to be absorbed. First the absorption coefficient increases rapidly below 0.050 Mev. In fact, at 0.010 Mev μ is greater than 24 times the value of μ at 0.050 Mev. Because of this, a photon with $E <$ 0.050 Mev will travel only a short distance before its next collision compared to a photon with $E > 0.050$ Mev.

Secondly, the probability that a collision will be an absorbing collision is more than 20 times greater at 0.010 Mev than at 0.050 Mev. In addition, a cobalt-60 photon has already lost 96 percent of its energy when it has an energy of 0.050 Mev. The above phenomena allows one to assume, without introducing appreciable error in the amount of energy absorbed, that whenever $\lambda_{n+1} > 10.22$ Compton units the photon is absorbed at the position of the n-th collision.

Since the position of the n-th collision is known, the program is used to calculate energy absorbed per unit volume, in mev/cm^3, on the n-th collision by

$$\frac{m(\Delta E_n)^{\ell}_i}{m(V_n)^{\ell}_i} \quad .$$

Change in Direction

The relation between the change in wave length and the scattering angle for Compton scattering is given by

$$\lambda_{n+1} - \lambda_n = 1 - \cos\ \theta_n$$

or

$$\theta_n = \cos^{-1}\ (1 - \lambda_{n+1} + \lambda_n) \quad .$$

Since all azimuthal angles are equally probable, the azimuthal scattering angle χ_n is determined by

$$\chi_n = 2\pi q \qquad \text{where} \qquad q \text{ is random on } (0,1)$$

The angle of the photon direction, referenced to the position of the n-th collision, with deflection angles θ_n and χ_n is

$$\vartheta_{n+1} = \cos^{-1}\ (\cos \vartheta_n \cos\ \theta_n + \sin\ \vartheta_n \sin\ \theta_n \cos\ \chi_n)$$

where $\vartheta_{n+1} = \cos^{-1}\ (\vec{\omega}_{n+1} \cdot \vec{j})$

and $\phi_{n+1} = \phi'_n + \cos^{-1}\ \left(\dfrac{\cos\ \theta_n - \cos \vartheta_n \cos \vartheta_{n+1}}{\sin \vartheta_n \sin \vartheta_{n+1}} \right)$

where $\phi_{n+1} = \cos^{-1}\ \left(\dfrac{\vec{\omega}_{n+1} \cdot \vec{i}_n}{\sin\ \vartheta_{n+1}}\right)$.

However, one wishes to reference the direction of the photon after the n-th collision, not to radial and axial vectors through the position of the n-th collision, but rather to the radial and axial vectors through the position of the (n+1) st collision. That is, one desires

$$\phi'_{n+1} = \cos^{-1}\left(\frac{\vec{\omega}_{n+1} \cdot \vec{i}_{n+1}}{\sin \vartheta_{n+1}}\right) \quad .$$

Obviously, the position of the (n+1) at collision must be determined before this can be accomplished. It is shown in Appendix B that

$$\phi'_{n+1} = \cos^{-1} \frac{r_{n+1}^2 + r_n^2 + (\xi_n \sin \vartheta_{n+1})^2}{2r_{n+1}(\xi_n \sin \vartheta_{n+1})} \quad .$$

The flow diagram for the change in direction of the photon on the n-th collision is given in Figure 7. The angles ϑ_{n+1}, and ϕ_{n+1}, are needed to determine the change in position. ϕ'_{n+1} is calculated in the subroutine Change in Position.

Change in Position

In order to determine the change in position it is necessary to know whether the photon passes through the duct. Since the duct consists of a void, the distance between the n-th and the (n+1)st collision will, on the average, be greater for photons passing through the duct than for those not passing through the duct. Thus, the generalized exponential distribution function for the distance between collisions

$$f(\xi_n)_m = \mu e^{-\mu(\xi_n)_m}$$

can be used only to determine the length of path of the photon through the shielding medium $(\xi_n)_m$. It is shown in Appendix B that the length of path through the void, $\bar{\xi}_n$ is

$$\bar{\xi}_n = \frac{2[R - r_n^2 \sin^2 \phi_{n+1}]^{\frac{1}{2}}}{\sin \vartheta_{n+1}} \quad .$$

Therefore, the total distance between collisions ξ_n is

$$\xi_n = \bar{\xi}_n + (\xi_n)_m$$

Figure 7. Flow diagram of change in direction subroutine

Input parameters = $\Delta\lambda_n$, ι_n, λ_n, φ'_n

Output parameters = ι_{n+1}, φ_{n+1}

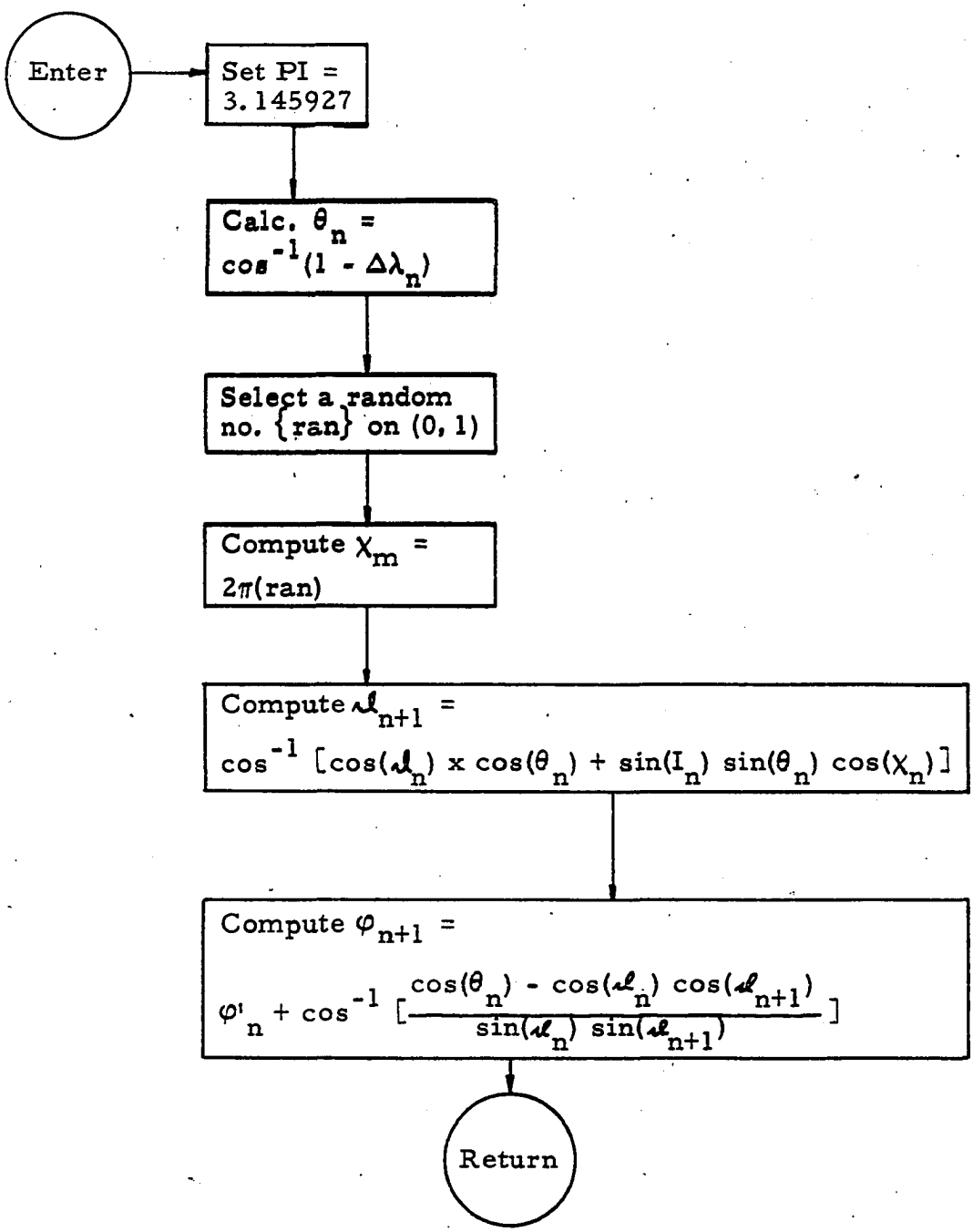

where $\bar{\xi}_n$ = o if the photon does not pass through the void. The position coordinates are given by

$$x_{n+1} = x_n + \xi_n \cos \vartheta_{n+1}$$

and

$$r_{n+1} = \sqrt{r_n^2 + (\xi_n \sin \vartheta_{n+1})^2 - 2r_n \xi_n \sin \vartheta_{n+1} \cos \phi_{n+1}}$$

Figure 8 gives the flow diagram for the change in position subroutine.

Figure 8. Flow diagram of change in position subroutine

Input parameters = μ_t, φ_{n+1}, ℓ_{n+1}, x_n, r_n, λ_{n+1}

Output parameters = φ'_{n+1}, r_{n+1}, x_{n+1}, INDIC

INDIC = 0 => Photon lost

INDIC = 1 => Photon not lost

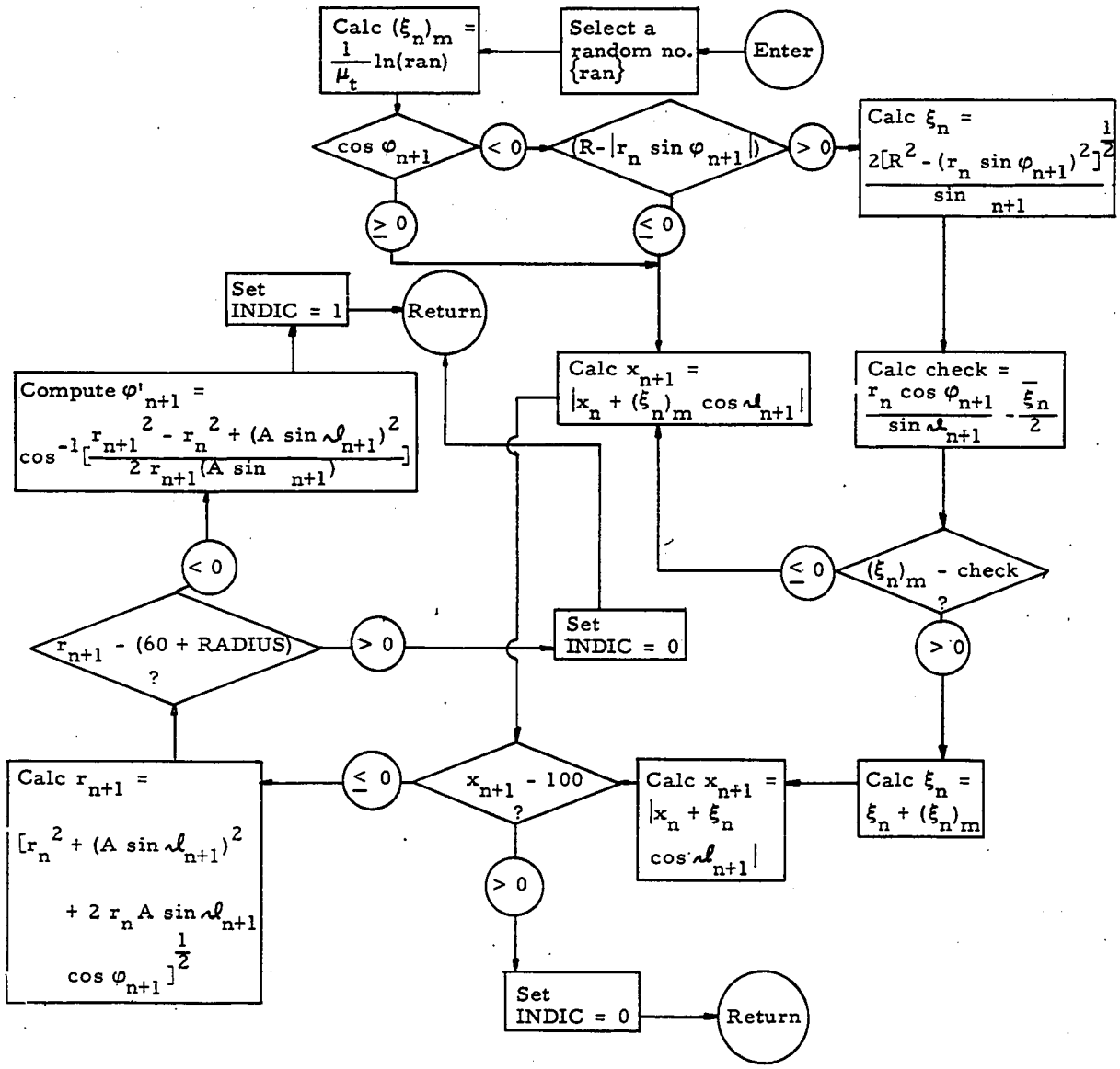

DISCUSSION OF RESULTS

Data Obtained

The solid lines of Figures 9, 10, 11, 13, 14, 16, 17, 19 and 21 are curves of the data obtained from the program. In order to facilitate differentiating between the data for adjacent curves in Figures 10, 11, 14, 17, 19 and 21, the symbols representing the data for adjacent curves are alternated between a circle and a triangle.

The solid lines of Figures 9, 10, and 11 are curves of the data obtained for the rate at which energy is absorbed in the no-void (i.e. R = 0) case. The dash-dot lines of Figures 9, 10, 11 and 12 give the rate at which energy is absorbed in an infinite homogeneous water medium. These curves were computed by integrating the photon spectrum given in NYO 3075 (24) for a point isotropic source of cobalt-60. The spectrum was normalized to a strength of 1 disintegration per second and the weight factor μ_a, the linear energy absorption coefficient, given in NBS 583 (25) was used in the integration. Since the photon spectrum given in NYO 3075 was for distances greater than 1 mfp (15.8 cm) of the primary photons, and well known analytic approximation to the buildup factor (26)

$$Ba = A_1 e^{-\alpha_1 \mu_o r} + (1 - A_1) e^{-\alpha_2 \mu_o r}$$

was used to compute the energy absorption rate for distances less than 1 mfp.

The curve with the two dots in Figure 12 gives the rate at which energy is absorbed in the homogeneous water shield due to the uncollided

photon flux.

The curves in Figures 13, 14, 16, 17, 19, and 21 are of the data obtained for the energy absorption rate, in the vicinity of the surface of the medium, as a function of distance from the medium-void interface in the direction perpendicular to the centerline of the void. The solid lines of Figures 12, 15, 18, 20 and 22 give the energy absorption rate at the surface of the medium-void interface as a function of the component of the distance from the source along the centerline of the void. The data for these curves were obtained by extrapolating the solid line curves of Figures 9, 10, 11, 13, 14, 17, 19 and 21 one-half of a centimeter to the surface.

The curves with two dots in Figures 15, 18, 20 and 22 give the energy absorption rate, at the surface of the medium-void interface, due to the uncollided flux, as a function of the component of the distance from the source along the centerline of the void. These curves were computed by the equation (Appendix C)

$$\mu_a(\lambda_o)\, I_o^o(r, \lambda_o) = \frac{\mu_a(\lambda_o)\, E_o \sin^3(\tan^{-1}\frac{R}{x})}{2\pi R^2}$$

where

$I_o^o(r, \lambda_o)$ = the energy flux of uncollided photons

$\mu_a(\lambda_o)$ = the energy absoption coefficient

E_o = the energy of the uncollided photons.

Accuracy of Data Near Medium-Void Interface

The energy absorption rate as a function of position in a water cylinder 60 cm in radial thickness and 200 cm in length was obtained from the

Figure 9. Energy absorption rate as a function of distance from centerline

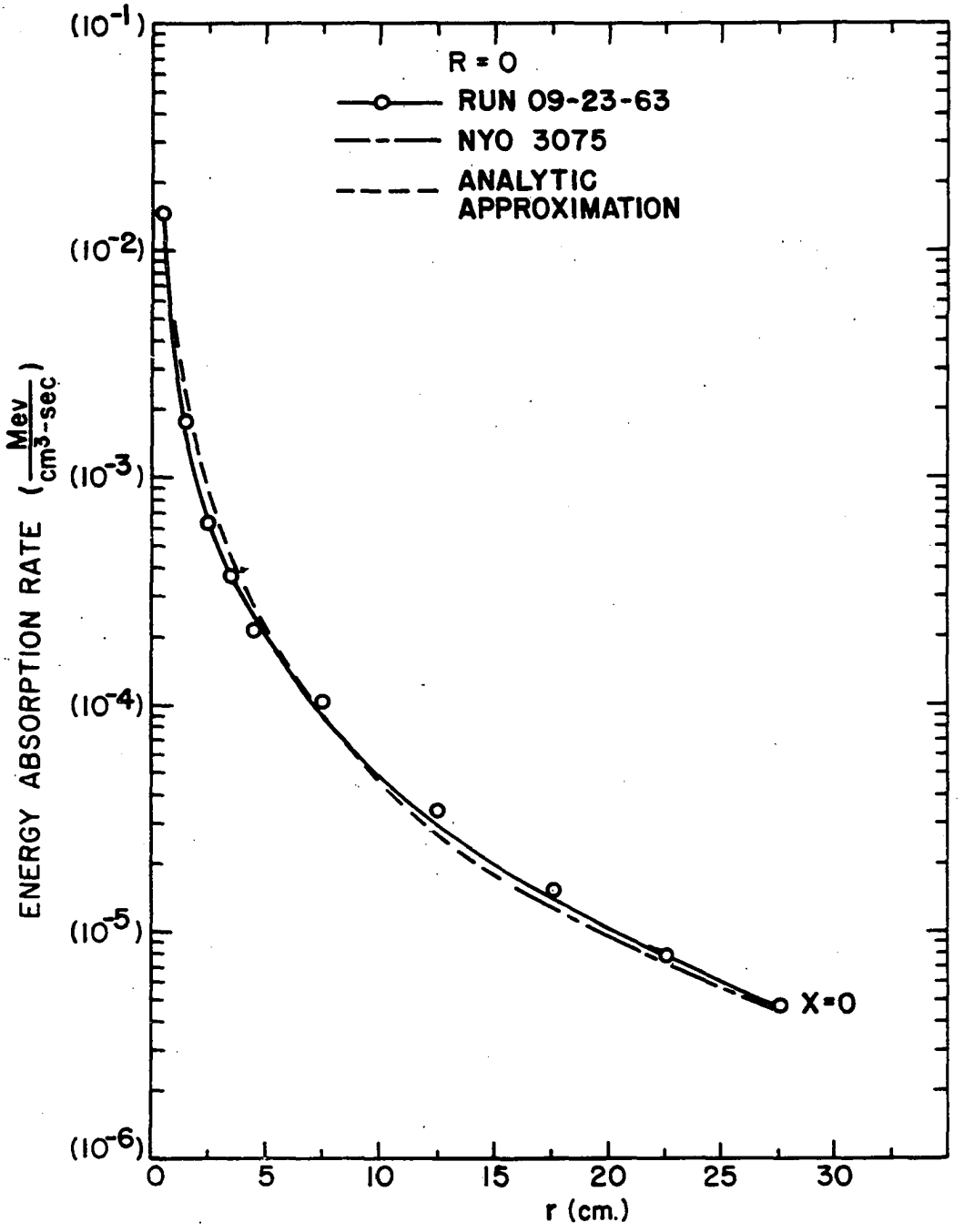
R = 0
RUN 09-23-63
NYO 3075
ANALYTIC APPROXIMATION
X=0
ENERGY ABSORPTION RATE (Mev / cm³-sec)
(10⁻¹)
(10⁻²)
(10⁻³)
(10⁻⁴)
(10⁻⁵)
(10⁻⁶)
0
5
10
15
20
25
30
r (cm.)

Figure 10. Energy absorption rate as a function of distance from centerline

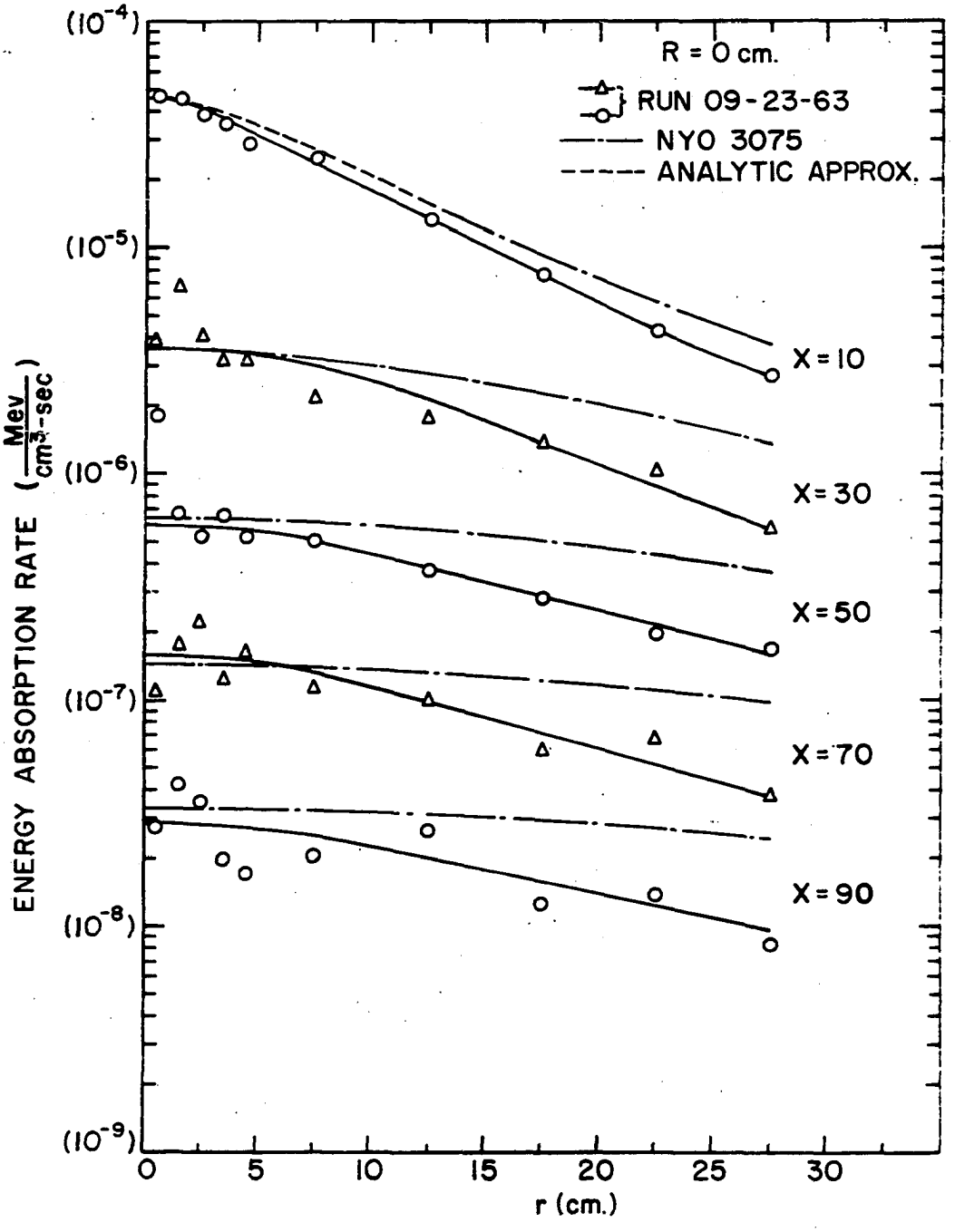
R = 0 cm.
RUN 09-23-63
NYO 3075
ANALYTIC APPROX.
X = 10
X = 30
X = 50
X = 70
X = 90
ENERGY ABSORPTION RATE (Mev / cm³-sec)
(10⁻⁴)
(10⁻⁵)
(10⁻⁶)
(10⁻⁷)
(10⁻⁸)
(10⁻⁹)
0
5
10
15
20
25
30
r (cm.)

Figure 11. Energy absorption rate as a function of distance from centerline

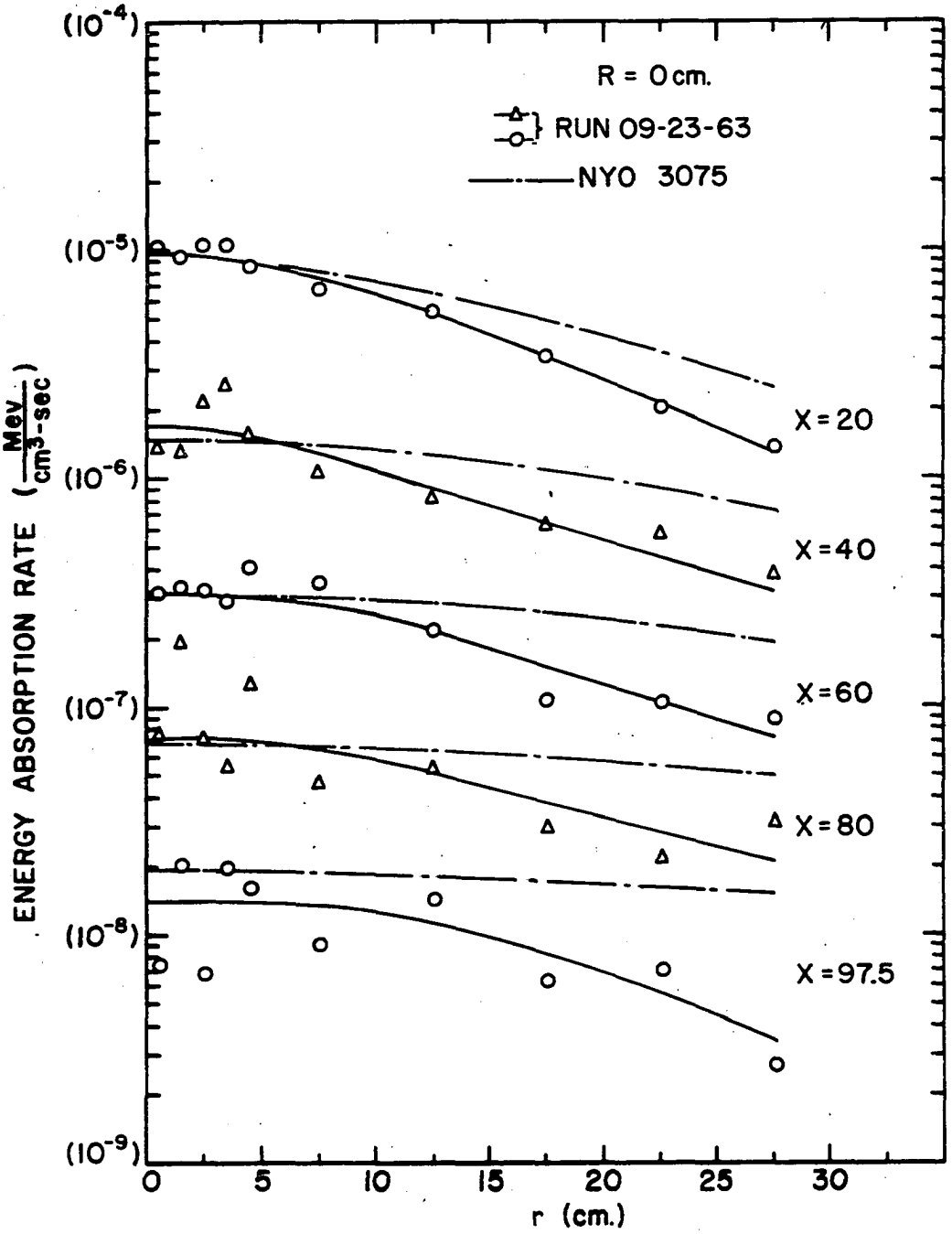
R = 0 cm.
RUN 09-23-63
NYO 3075
X = 20
X = 40
X = 60
X = 80
X = 97.5
ENERGY ABSORPTION RATE (Mev / cm³-sec)
(10⁻⁴)
(10⁻⁵)
(10⁻⁶)
(10⁻⁷)
(10⁻⁸)
(10⁻⁹)
0
5
10
15
20
25
30
r (cm.)

Figure 12. Energy absorption rate at interface as a function of distance along centerline

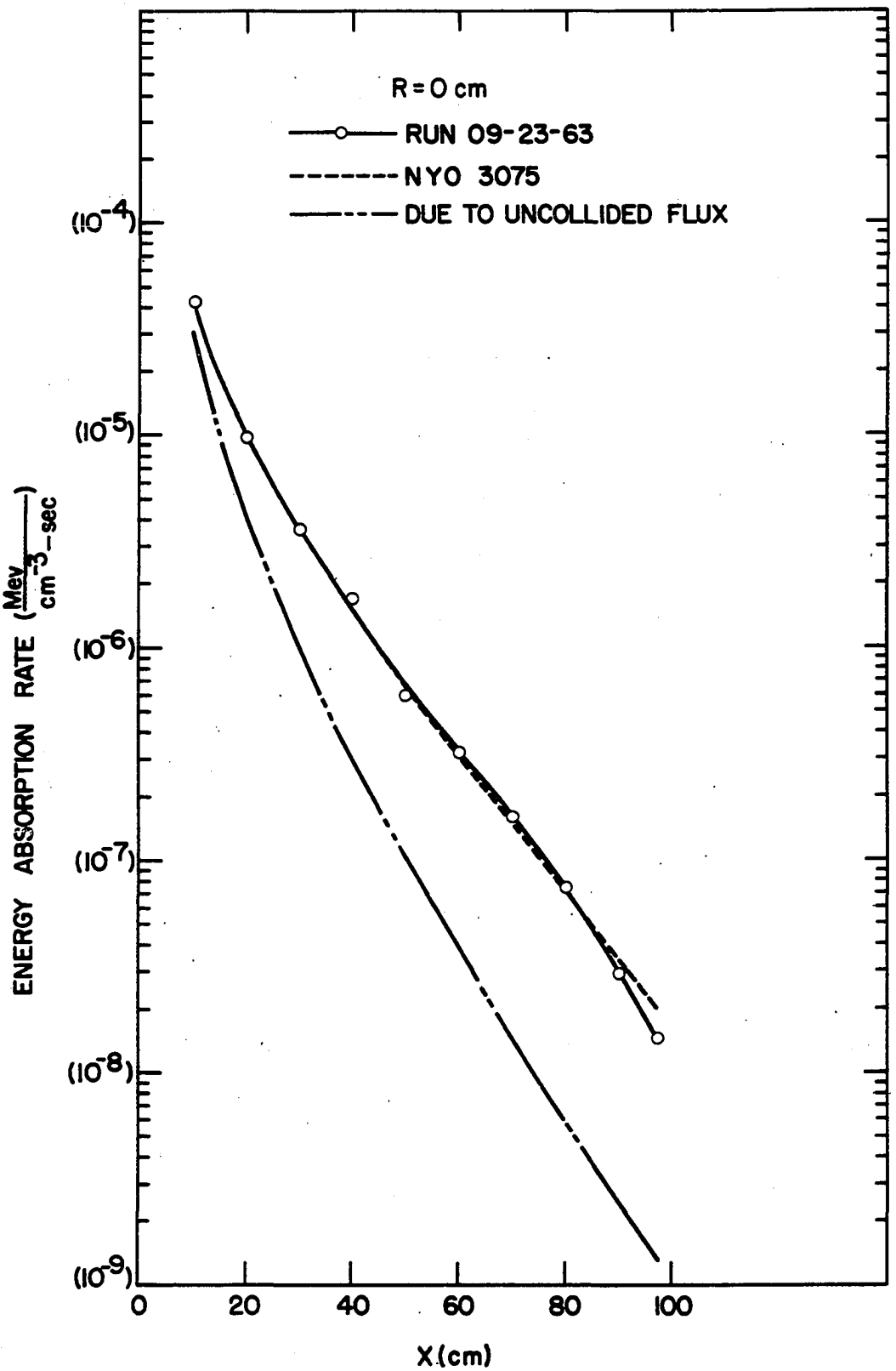
R = 0 cm
RUN 09-23-63
NYO 3075
DUE TO UNCOLLIDED FLUX
ENERGY ABSORPTION RATE (Mev / cm⁻³-sec)
(10⁻⁴)
(10⁻⁵)
(10⁻⁶)
(10⁻⁷)
(10⁻⁸)
(10⁻⁹)
0
20
40
60
80
100
X (cm)

Figure 13. Energy absorption rate as a function of distance from interface

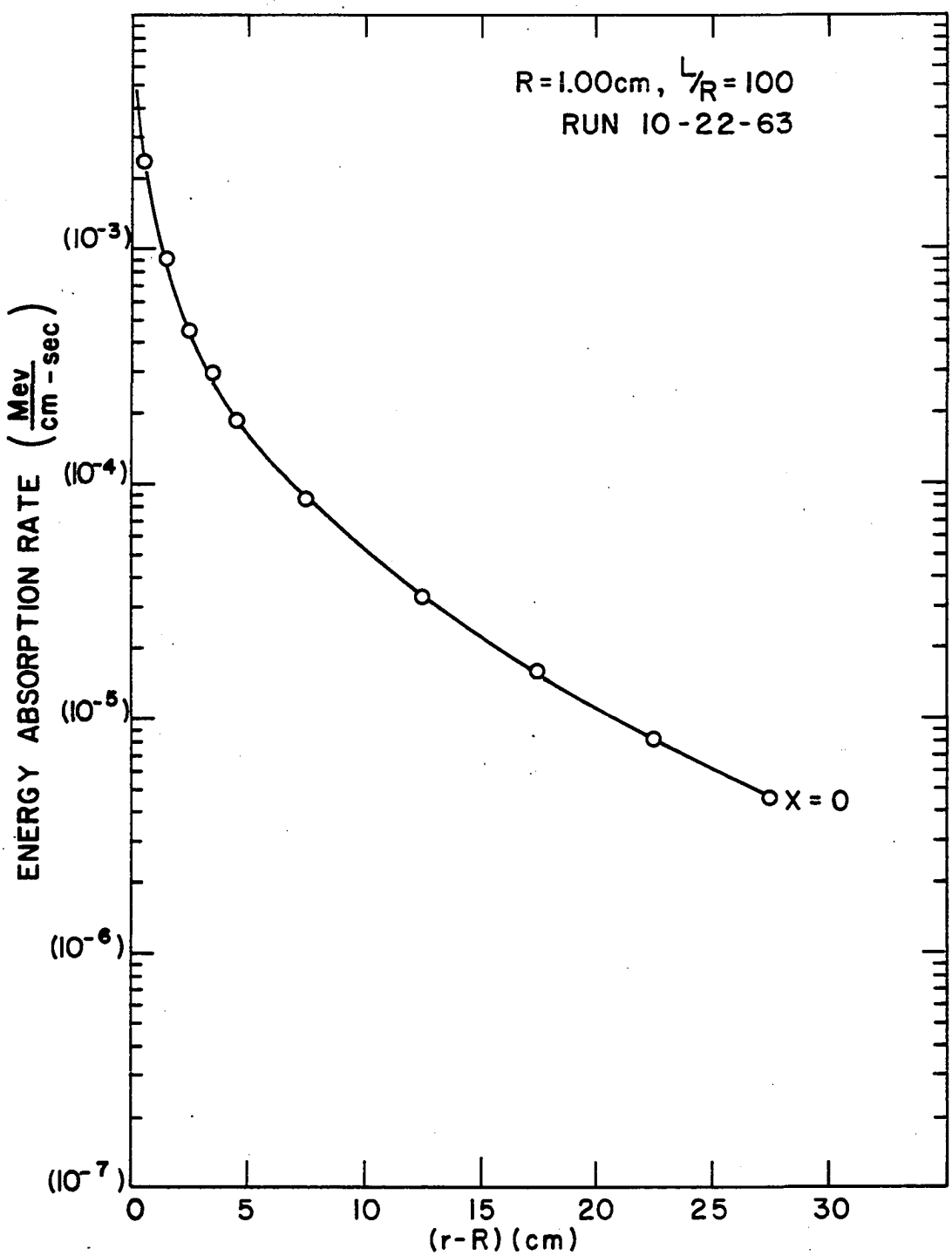
R = 1.00cm, L/R = 100
RUN 10-22-63
ENERGY ABSORPTION RATE (Mev / cm-sec)
(10⁻³)
(10⁻⁴)
(10⁻⁵)
(10⁻⁶)
(10⁻⁷)
X = 0
0
5
10
15
20
25
30
(r-R) (cm)

Figure 14. Energy absorption rate as a function of distance from interface

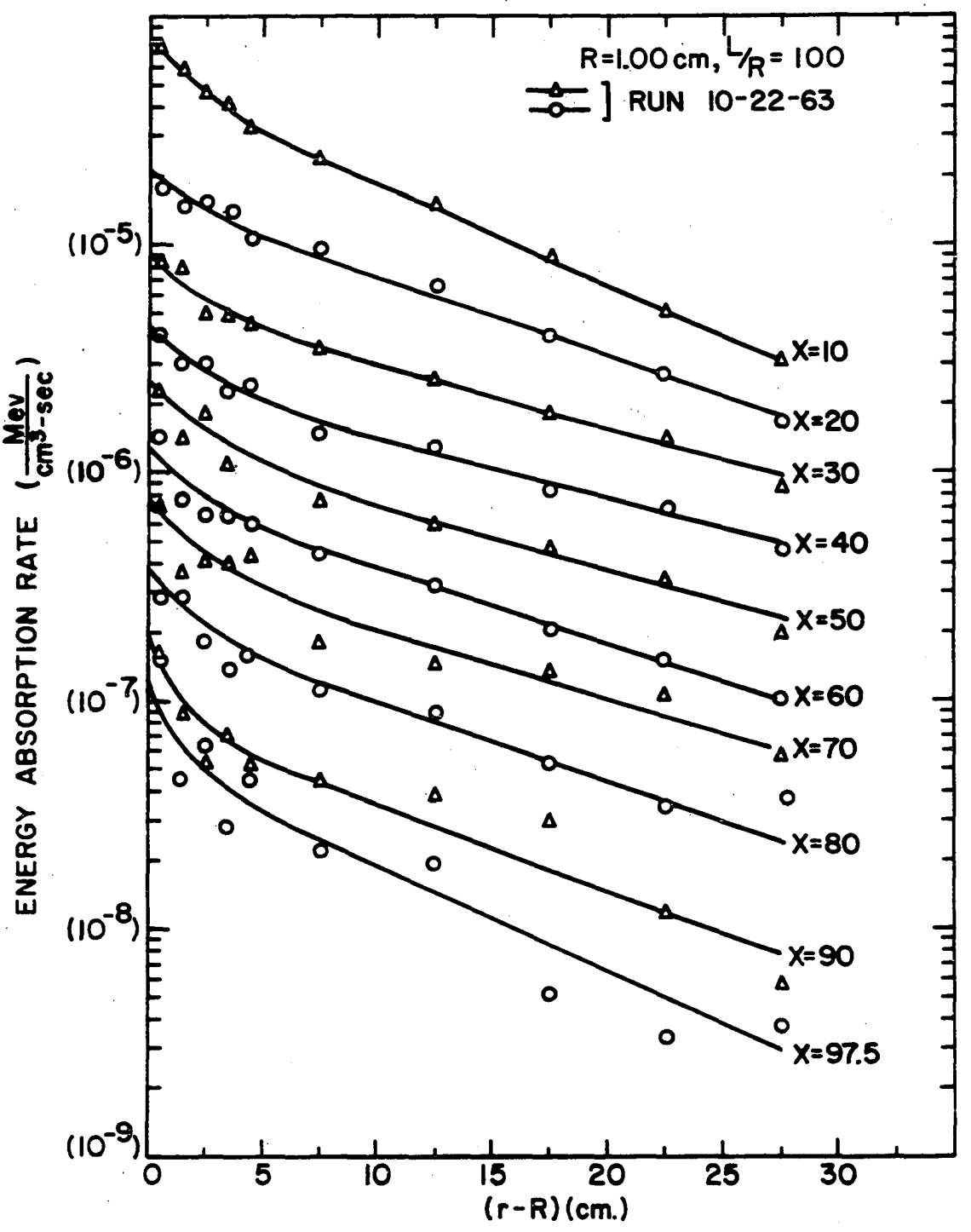
R=1.00 cm, L/R = 100
RUN 10-22-63
X=10
X=20
X=30
X=40
X=50
X=60
X=70
X=80
X=90
X=97.5
ENERGY ABSORPTION RATE (Mev / cm3-sec)
(10-5)
(10-6)
(10-7)
(10-8)
(10-9)
0
5
10
15
20
25
30
(r-R)(cm.)

Figure 15. Energy absorption rate at interface as a function of distance along centerline

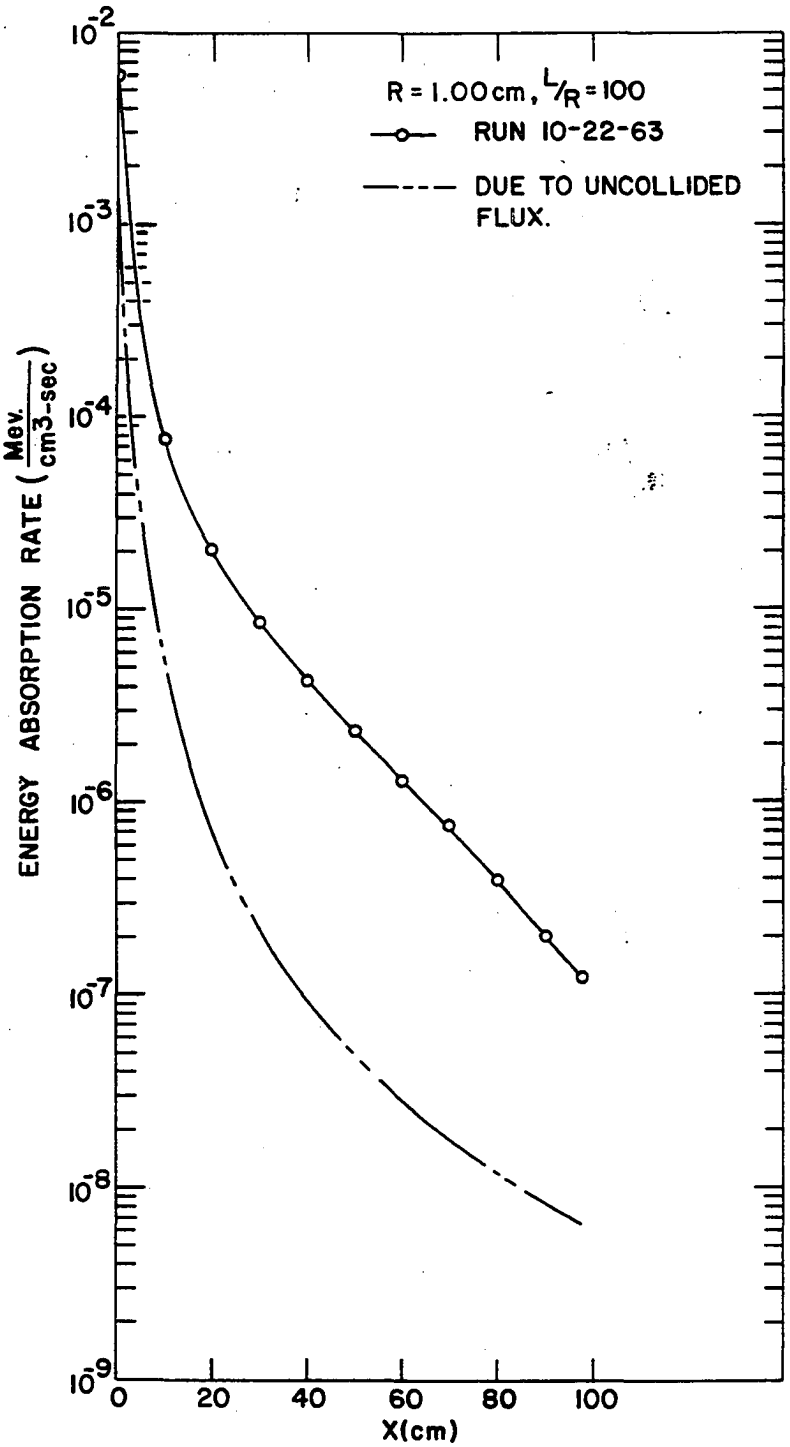
R = 1.00 cm, L/R = 100
RUN 10-22-63
DUE TO UNCOLLIDED FLUX.
ENERGY ABSORPTION RATE (Mev./cm3-sec)
10-2
10-3
10-4
10-5
10-6
10-7
10-8
10-9
0
20
40
60
80
100
X(cm)

Figure 16. Energy absorption rate as a function of distance from interface

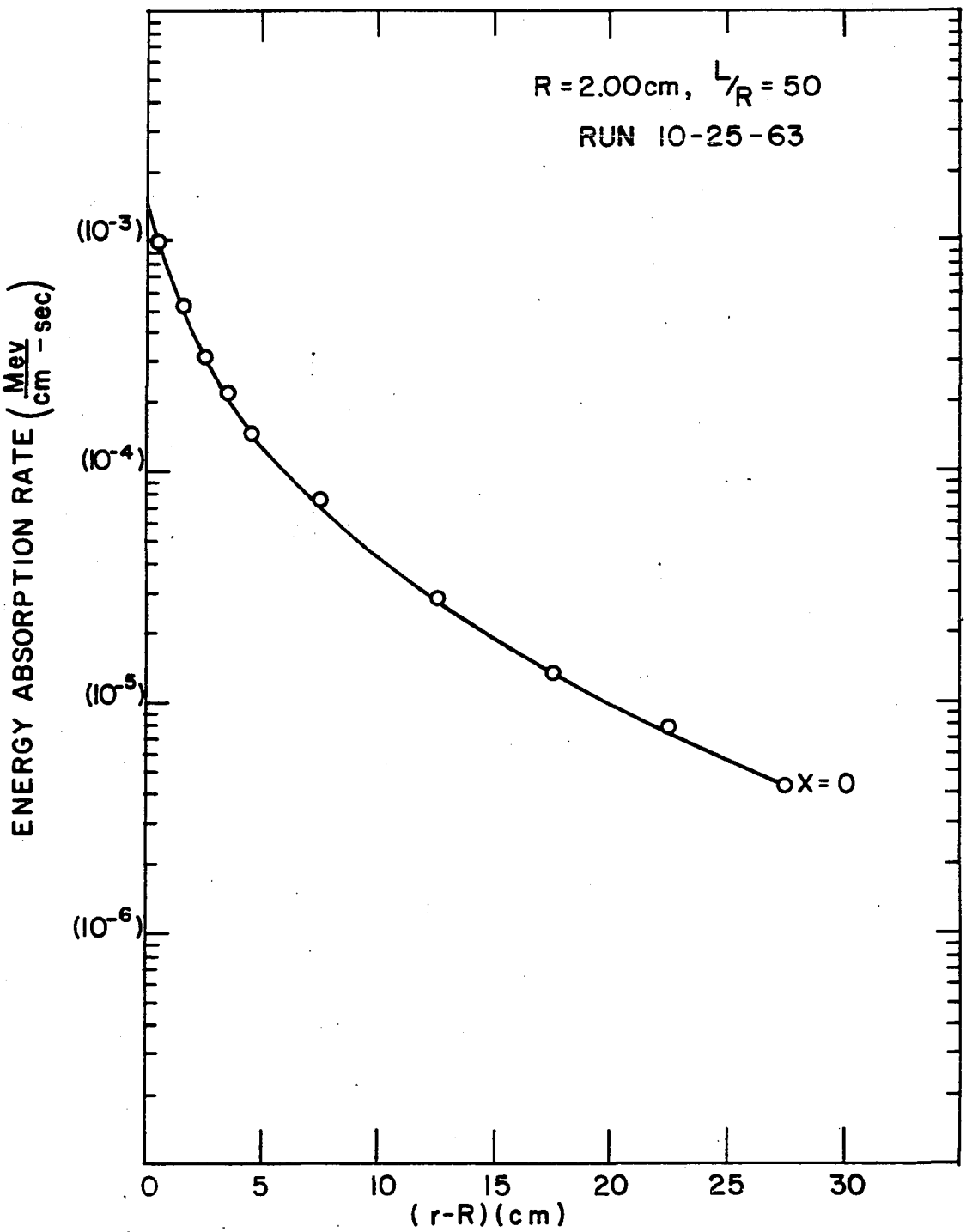
R = 2.00cm, L/R = 50
RUN 10-25-63
ENERGY ABSORPTION RATE (Mev / cm - sec)
(10⁻³)
(10⁻⁴)
(10⁻⁵)
(10⁻⁶)
X = 0
0
5
10
15
20
25
30
(r-R)(cm)

Figure 17. Energy absorption rate as a function of distance from interface

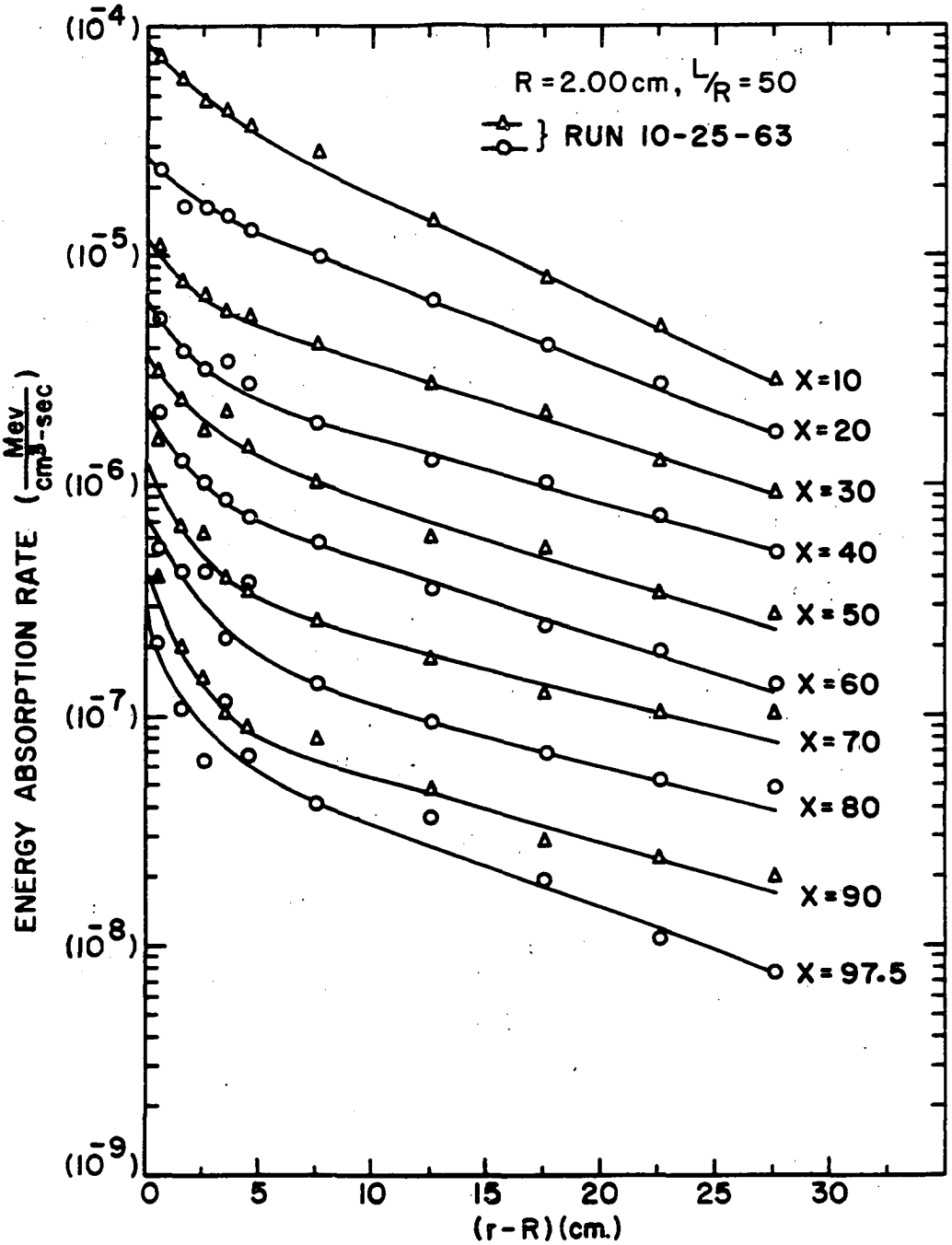
R = 2.00 cm, L/R = 50
RUN 10-25-63
X=10
X=20
X=30
X=40
X=50
X=60
X=70
X=80
X=90
X=97.5
ENERGY ABSORPTION RATE (Mev / cm³-sec)
(10⁻⁴)
(10⁻⁵)
(10⁻⁶)
(10⁻⁷)
(10⁻⁸)
(10⁻⁹)
0
5
10
15
20
25
30
(r-R) (cm.)

Figure 18. Energy absorption rate at interface as a function of distance along centerline

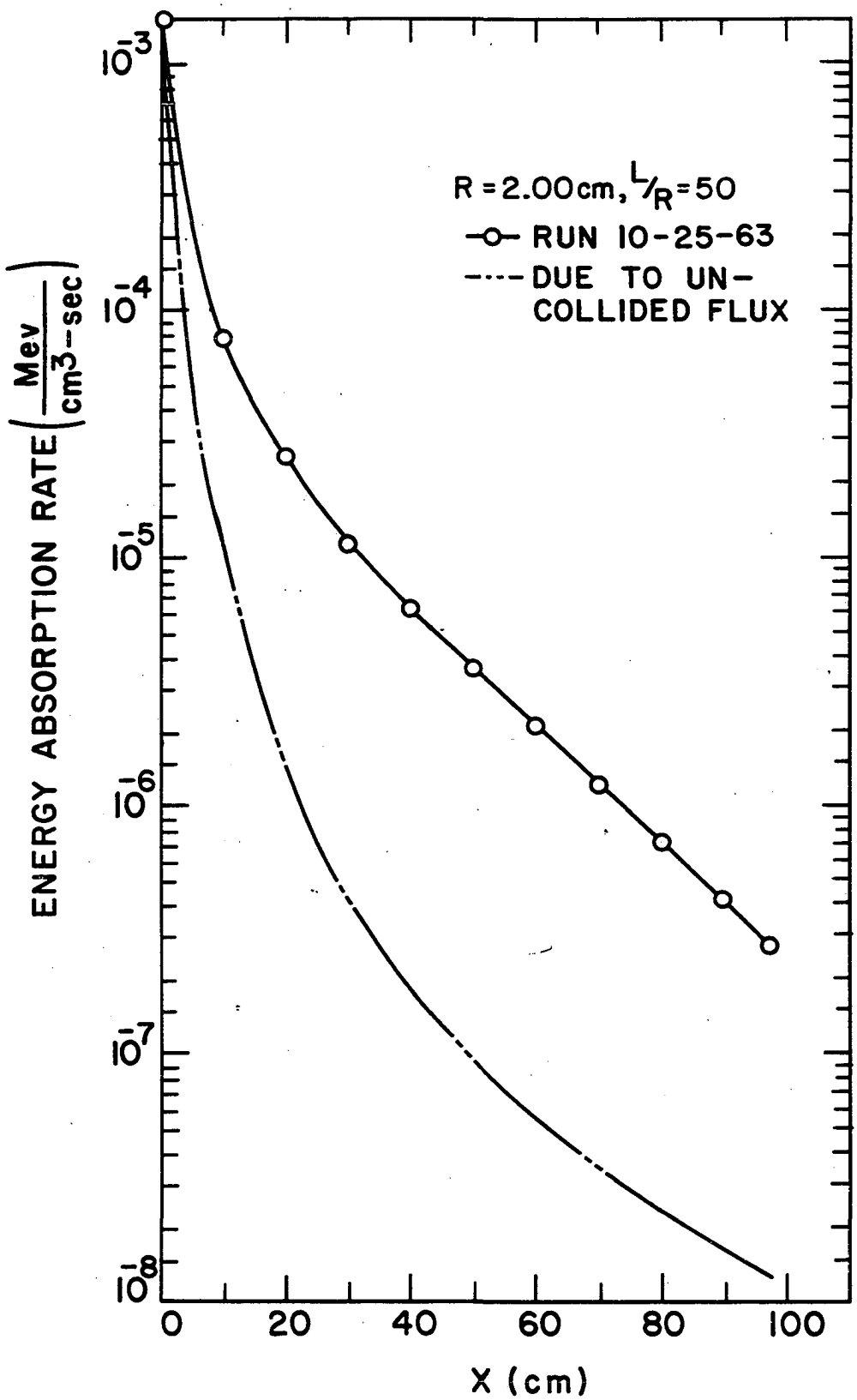
R = 2.00cm, L/R = 50
RUN 10-25-63
DUE TO UN-COLLIDED FLUX
ENERGY ABSORPTION RATE (Mev / cm3-sec)
10-3
10-4
10-5
10-6
10-7
10-8
0
20
40
60
80
100
X (cm)

Figure 19. Energy absorption rate as a function of distance from interface

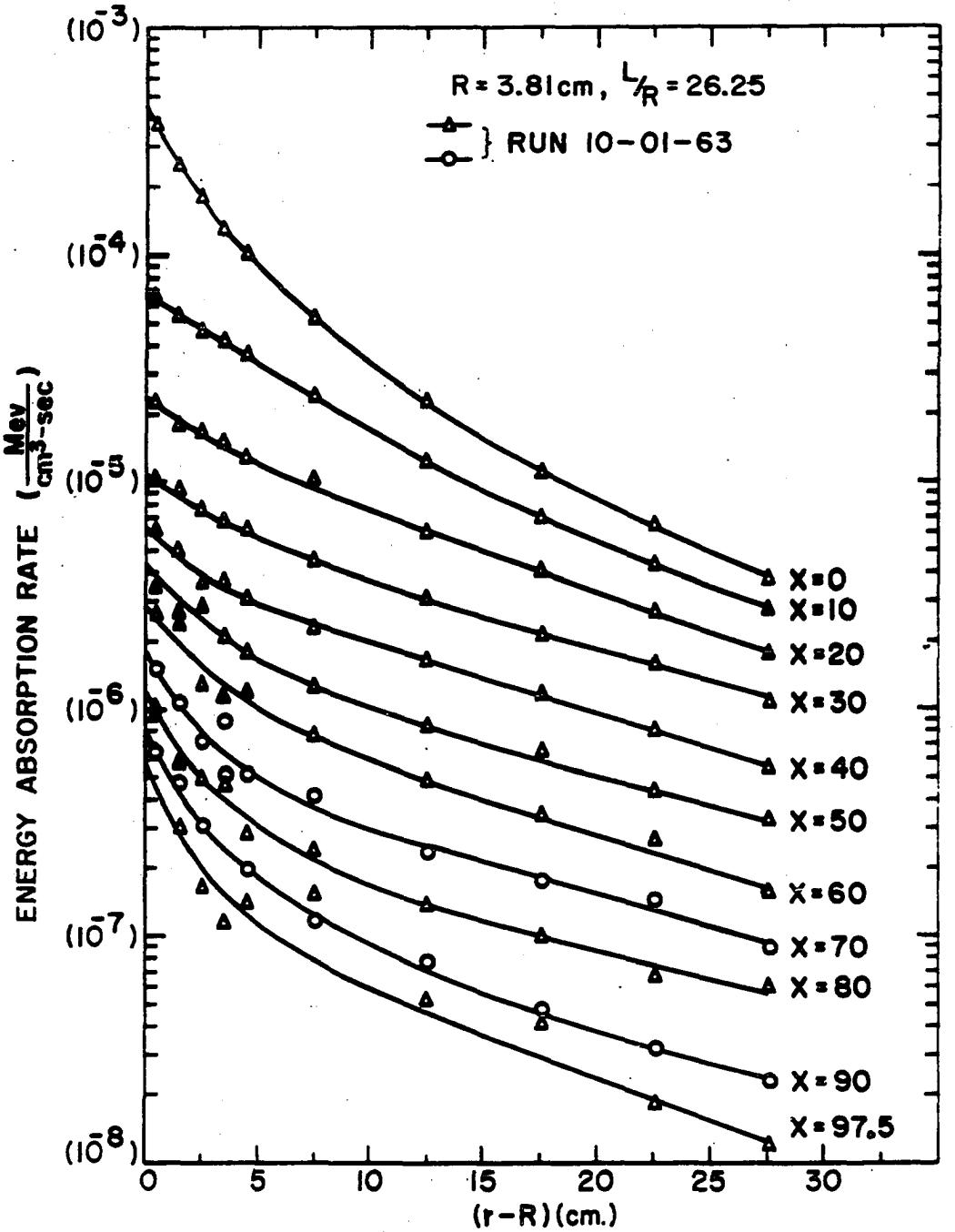
R = 3.81cm, L/R = 26.25
RUN 10-01-63
X=0
X=10
X=20
X=30
X=40
X=50
X=60
X=70
X=80
X=90
X=97.5
ENERGY ABSORPTION RATE (Mev / cm³-sec)
(10⁻³)
(10⁻⁴)
(10⁻⁵)
(10⁻⁶)
(10⁻⁷)
(10⁻⁸)
0
5
10
15
20
25
30
(r-R)(cm.)

Figure 20. Energy absorption rate at interface as a function of distance along centerline

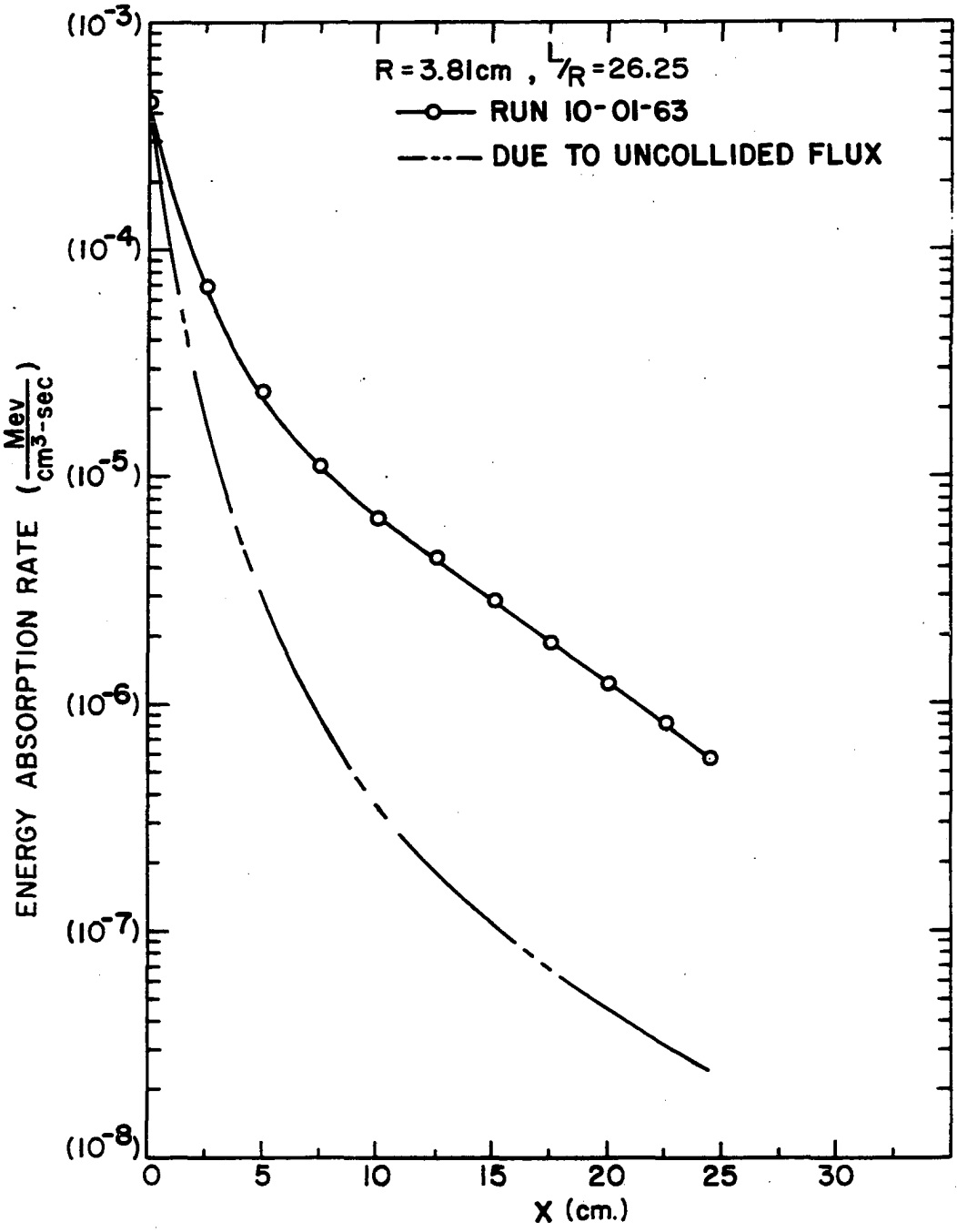
R = 3.81cm , L/R = 26.25
RUN 10-01-63
DUE TO UNCOLLIDED FLUX
ENERGY ABSORPTION RATE (Mev / cm³-sec)
(10⁻³)
(10⁻⁴)
(10⁻⁵)
(10⁻⁶)
(10⁻⁷)
(10⁻⁸)
0
5
10
15
20
25
30
X (cm.)

Figure 21. Energy absorption rate as a function of distance from interface

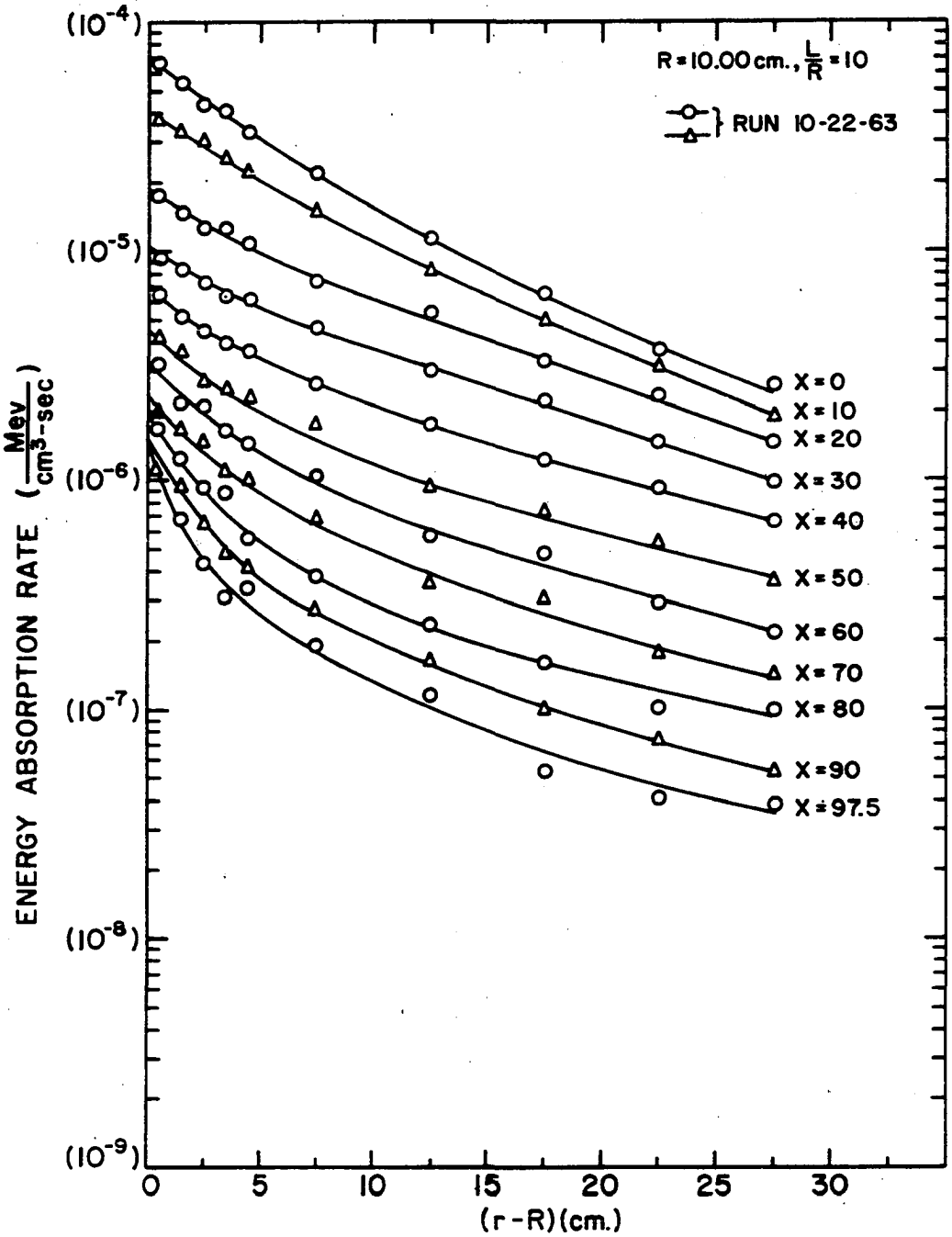
R = 10.00 cm., L/R = 10
RUN 10-22-63
X = 0
X = 10
X = 20
X = 30
X = 40
X = 50
X = 60
X = 70
X = 80
X = 90
X = 97.5
ENERGY ABSORPTION RATE (Mev / cm³-sec)
(10⁻⁴)
(10⁻⁵)
(10⁻⁶)
(10⁻⁷)
(10⁻⁸)
(10⁻⁹)
0
5
10
15
20
25
30
(r - R)(cm.)

Figure 22. Energy absorption rate as a function of distance along centerline

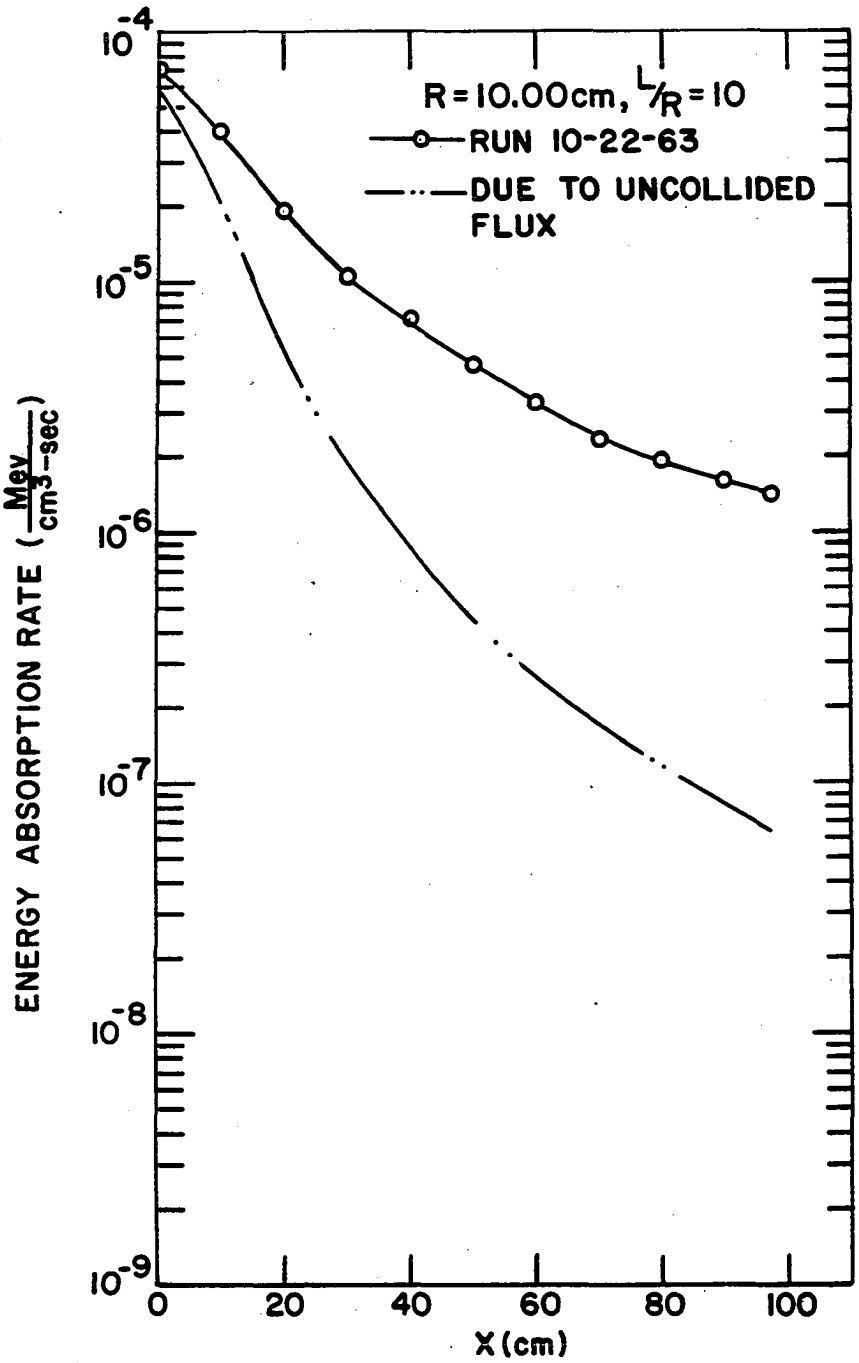
R = 10.00cm, L/R = 10
RUN 10-22-63
DUE TO UNCOLLIDED FLUX
ENERGY ABSORPTION RATE (Mev/cm³-sec)
10⁻⁴
10⁻⁵
10⁻⁶
10⁻⁷
10⁻⁸
10⁻⁹
0
20
40
60
80
100
X (cm)

program. It was observed that the initial collisions, which occured in a 5 cm thick cylindrical volume symmetric with the centerline and having an inside radius 20 cm greater than the radius of the void, contributed approximately 10 percent of the energy that was absorbed 1/2 cm from the void-medium interface. The initial collisions that occurred in the 5 cm thick cylinder having an inside radius of 25 cm greater than the radius of the void contributed approximately 1 percent of the energy that was absorbed 1/2 cm from the interface. It is therefore assumed that no significant information about the energy absorption rate at the interface between the medium and the void can be obtained by having initial collisions occur at a distance greater than 27.5 cm (almost 2 mfp) from the interface. For this reason no photons were assumed to have an initial collision at a distance greater than 27.5 cm from the interface. Consequently the rate at which energy is absorbed as determined by this investigation should be less than the rate for an infinitely thick cylinder at all positions except for those at the void-medium interface where the rates should coincide. No attempt is made to determine the actual energy absorption rate in the medium at any positions except those at the medium-void interface.

One notes from Figure 9 that the deviation of the data points from the R = 0 (i.e. no void), x = o curve, as this curve approaches the centerline of the shield, is nil. However Figure 11 shows that the average deviation of the last five data points from the R = 0, x = 97.5 cm curve, as this curve approaches the centerline, is 28 percent. Figures 14, 17, 19 and 21 show that the deviation of the data points

from the curves near the void decreases as the size of the void increases, but for any size void, the deviation increases as distance from the source along the centerline of the void increases.

This can best be explained by considering first the no-void case. A photon which has only a glancing initial collision (no loss in energy or change in direction) near the source has the same probability of having its second collision 97.5 cm from the source as a source photon has of having its initial collision 97.5 cm from the source. The scattered photon, however, has the weight factor determined by the position of its initial collision which, if the initial collision occurs at less than 10 cm from the source, will be more than (10^3) times the weight factor of the source photon which has its initial collision 97.5 cm from the source.

The probability of a photon having an initial glancing collision near the source and its second collision 97.5 cm from the source is extremely small, but when it occurs, the program (and correctly so) will cause the photon to deposit more than (10^3) times the energy per collision as a source photon whose initial collision was 97.5 cm from the source. At 97.5 cm from the source, therefore, the rate at which energy is absorbed will not be as smooth a function of position as when it is nearer the source. Similarly whenever the initial weight factors between two points in a medium differ greatly, the prediction made by this program of the rate at which energy is absorbed will be least accurate for the position with the smallest initial weight factor.

Using 20,000 photons for the no-void run where the initial weight

factors differed by approximately (10^6) between 1/2 cm from the source and 97.5 cm from the source, the data near the centerline, 97.5 cm from the source, appears to have an average deviation of 28 percent (Figure 11). Using 22,000 photons for the 10 cm radius void run where the maximum difference in weight factors along the surface of the medium is (10^3), the average deviation near the surface of the void is less than 1 percent (Figure 21).

The accuracy can be increased, of course, by using more histories. Such an increase was not justified for this investigation, however, since the greatest inaccuracy in the rate at which the energy is absorbed at a void-medium interface will occur at 97.5 cm from the source in the shield that has the void with the smallest radius. The smallest radius void investigated was a 1-cm radius void, where, due to the deviation of the data points, the error was approximately 10 percent when 22,000 histories were used (Figure 14). Partial runs were made to indicate the expected deviation of the data points as a function of the number of photon histories. It was concluded that perhaps 220,000 histories would be needed to reduce by one-third the error obtained when using 22,000 histories.

Data for Infinite Medium Compared to the Data from no Void Run

The rate at which energy is absorbed along the centerline of the cylinder as obtained by this investigation is compared in Figure 12 to the rate predicted for an infinite medium. A maximum error of less than 5 percent occurs at 70 cm from the source. At 97.5 cm from the source the

rate obtained was 32 percent below the rate for an infinite medium because a boundary between the medium and a void was assumed to exist along a plane perpendicular to the centerline and 100 cm from the source. Therefore no photons that cross this boundary could return to contribute to the energy absorbed at 97.5 cm from the source.

Kays' Data Compared to the Data
from the 3.81 cm Radius Duct Run

The rate at which energy is absorbed in water surrounding an air duct of 3.81 cm in radius as reported by Kays (27) is compared in Figure 23 to the rate obtained for a duct of 3.81 cm in radius by this study. Kays' observations were made in the shield tank of the UTR-10 reactor at Iowa State University. The shield tank has a 5 foot by 6 foot cross section and was filled with water to a depth of 11 1/2 feet. Kays placed an aluminum duct 3.81 cm in diameter, 9 feet long and 57 mils thick in the shield tank and obtained the rate at which energy is absorbed in the water surrounding the duct. His source of radiation was 1.15 mc of cobalt-60 placed along the centerline of the duct midway between the ends.

The experimental facility utilized by Kays therefore differs from the experimental facility assumed by the author in that

a. Kays' duct contained air while the author assumed a void.

b. the aluminum duct was 57 mils thickness while the author assumed no material between the void and the water.

c. the UTR-10 shield tank had a minimum of 150 cm of water surrounding the duct while the author assumed only 60 cm.

d. Kays used a 1.15 mc source while the author assumed a source of

Figure 23. Energy absorption rate as a function of distance from interface

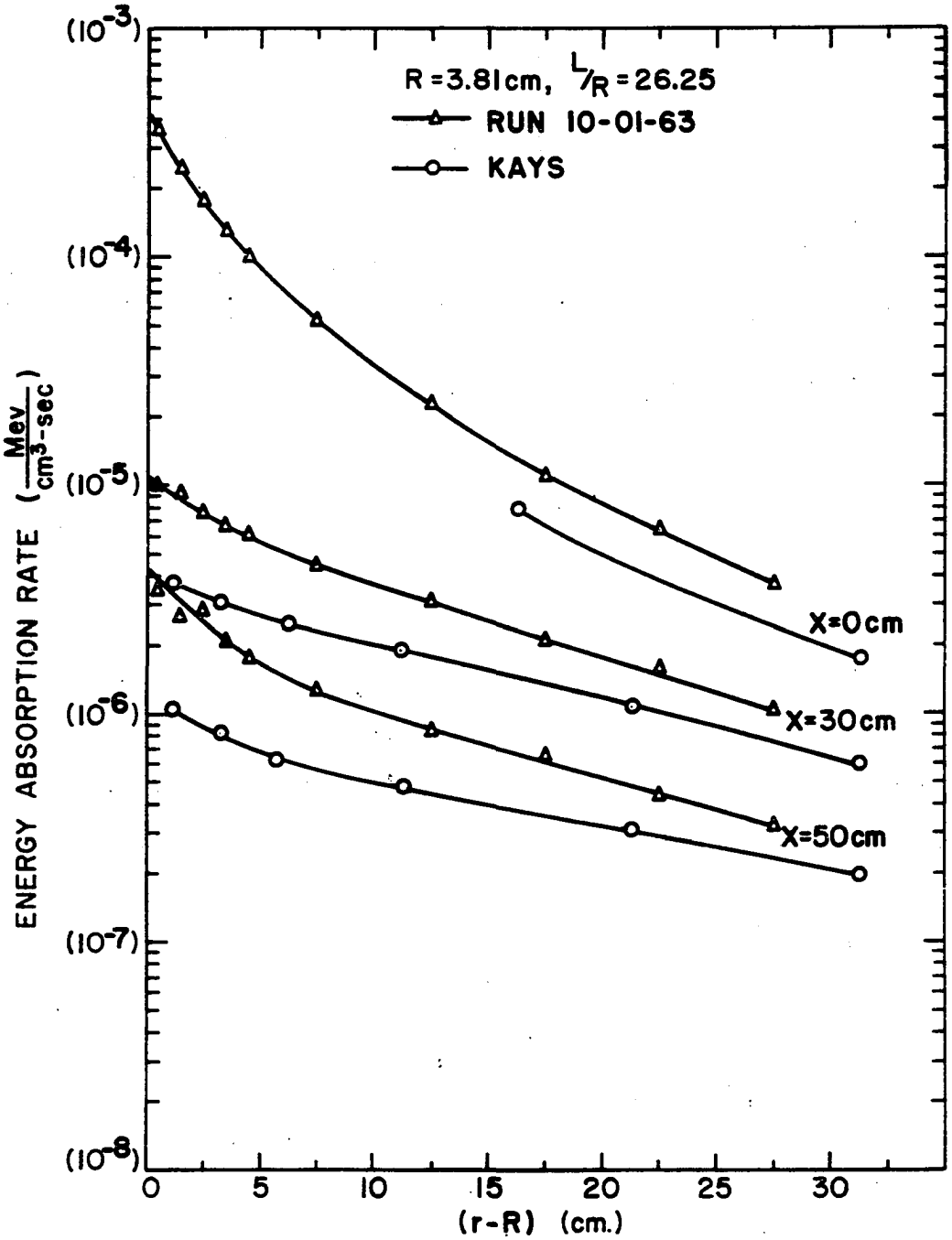
R = 3.81cm, L/R = 26.25
RUN 10-01-63
KAYS
X=0cm
X=30cm
X=50cm
ENERGY ABSORPTION RATE (Mev / cm³-sec)
(10⁻³)
(10⁻⁴)
(10⁻⁵)
(10⁻⁶)
(10⁻⁷)
(10⁻⁸)
0
5
10
15
20
25
30
(r-R) (cm.)

1 disintegration per second.

The differences noted in a and b are negligible. As mentioned earlier, scattering at a distance greater than 60 cm from the void would increase the rate of energy absorbed deep in the medium but would have a negligible effect on the rate of energy absorbed at the medium-void interface. Thus Kays data, normalized to 1 disintegration per second, should be similar to the author's at the surface and indicate a higher value than the author's as distance increases from the void.

By comparing the data Kays obtained without the duct at 30 cm from the source to values calculated from the buildup factors presented in Goldstein (7), he estimated that the shape of his curves were correct but that most of his data were from 20 percent to 25.7 percent low. One notes in Figure 23 that at X = 30 cm, Kays' data indicates a rate at which energy is absorbed, 1 cm from the void, that is only 40 percent of the author's value.

Approximately 33 percent of the rate at which energy is absorbed in water at a distance of 30 cm from a cobalt-60 source is due to the uncollided flux (i.e. high energy flux). Approximately 40 percent of the rate at which energy is absorbed 1 cm from the interface of a 3.81 cm radius void and 30 cm from the source is due to the uncollided flux. If one assumes, therefore, that Kays' experiment grossly underestimated the high energy flux, one might expect his data to be almost 30 percent below the actual value for the no void case and almost 40 percent below the author's value for the shield with a 3.81 cm radius void.

A verification of the assumption that Kays underestimated the high energy flux is found by examining the flux spectra obtained by Kays at a

position 30 cm from the source. Kays indicates that the flux at 1 Mev is 1.7 percent of the flux at 0.1 Mev, whereas NYO 3075 (24) indicates that the flux at 1 Mev should be 33 percent of the flux at 0.1 Mev. One therefore concludes that the difference in the energy absorption rate between the author's value and Kays' value, as is shown in Figure 23, is caused by an error in Kays' value.

Dimensional Analysis

Dimensional analysis is a tool which enables one to relate the pertinent variables through their fundamental dimensions, rather than through the numerical values of the variables. By applying dimensional analysis to physical phenomenon, dimensionless groups can be determined which are interrelated and which can be used to predict the results of changes in the magnitude of the dimensional variables comprising the dimensionless groups.

The Buckingham Pi Theorem provides a means of reducing the number of variables by grouping the variables into dimensionless groups called pi terms. The Buckingham Pi Theorem states that the number of independent pi terms, s, is equal to the number of variables concerned minus the number of fundamental dimensions required to express the variables (28). A functional relationship between the pi terms can then be expressed as

$$\pi_1 = F(\pi_2, \pi_3, \ldots \pi_s) \quad .$$

The basic variables generally assumed in determining the rate at which energy is absorbed, due to gamma radiation, in the vicinity of ducts in shields can be written in functional notation as

$${}_oD = f({}^o_oD, \mu_t(E_o), \mu_t(E), \mu_{sc}(E), R, L, x)$$

where $_{o}D$ is arbitrarily chosen as the dependent variable. A tabulation of the eight variables in terms of the dimensions of force (F), length (l) and time (T) is given in Table 1.

Table 1. Basic Variables

	Variables	Dimensions	Parameters
$_{o}D$	Rate at which energy is absorbed due to photons of all energies	$F\ l^{-2}T^{-1}$	source, material, geometric, energy of photon before i-th collision
$^{o}_{o}D$	Rate at which energy is absorbed due to uncollided photons	$F\ l^{-2}T^{-1}$	sources, material, geometry
$\mu_t(E_o)$	Total absorption coefficient of uncollided photons	l^{-1}	source, material
$\mu_t(E_i)$	Total absorption coefficient at energy E_i	l^{-1}	material, energy of photon before i-th collision
$\mu_{sc}(E_i)$	Scattering coefficient at energy E_i	l^{-1}	material, energy of photon before i-th collision
R	Radius of void	l	geometry
L	Length of void	l	geometry
x	Distance from source along centerline of void	l	geometry

Since $F\ l^{-2}T^{-1}$ is equally as basic a quantity (dimension) as force, length or time, one observes from Table 1 that the variables are expressed in terms of two dimensions, $F\ l^{-2}T^{-1}$ and l. The Buckingham Pi Theorem therefore predicts six independent pi terms. One possible selection of pi terms is presented in Table 2.

By using the pi terms listed in Table 2, the functional relationship between the dimensionless groups is

$$B_a = F\left(\mu_t(E_o)x,\ \mu_t(E_o)L,\ \frac{L}{R},\ \frac{\mu_t(E_i)}{\mu_t(E_o)},\ \frac{\mu_t(E_i)}{\mu_{sc}(E_i)}\right)$$

Table 2. Pi terms

Terms		Parameters
$\pi_1 = B_a = \frac{{}_oD}{{}_oD}$	Energy absorption buildup factor	source, material, geometry, energy of photon before i-th collision
$\pi_2 = \mu_t(E_o)x$	Distance from source in terms of mfp of uncollided photons	source, material, geometry
$\pi_3 = \mu_t(E_o)L$	Length of void (or thickness of shield) in terms of mfp of uncollided photons	sources, material, geometry
$\pi_4 = \frac{L}{R}$	Ratio of length to radius of void	geometry
$\pi_5 = \frac{\mu_t(E_i)}{\mu_t(E_o)}$	Ratio of total absorption coefficient at energy E_i to total absorption coefficient at source energy	source, material, energy of photon before i-th collision
$\pi_6 = \frac{\mu_{sc}(E_i)}{\mu_t(E_i)}$	Ratio of scattering to total coefficient at energy E_i	material, energy of photon before i-th collision

where B_a is arbitrarily chosen as the dependent pi term. A disadvantage of this selection of pi terms is that it is not possible to obtain numerical values for π_5, $\frac{\mu_t(E_i)}{\mu_t(E_o)}$, or π_6, $\frac{\mu_{sc}(E_i)}{\mu_t(E_i)}$. Nevertheless it is possible to determine the manner in which π_1 varies with π_2, π_3 and π_4,

the term that depend upon the geometry.

The variation of B_a as a function of $\mu_t(E_o)x$ at various values of $\frac{L}{R}$ is presented in Figure 24. An analysis of the curves of Figure 24 shows that the component equations obtained by varying $\mu_t(E_o)x$, $\mu_t(E_o)L$ and $\frac{L}{R}$ will not combine by either multiplication or addition to form the general prediction equation for B_a. Further dimensional analysis was felt to be beyond the scope of this investigation and was therefore not pursued.

Energy Absorption Buildup Factor B_a

The curves are various $\frac{L}{R}$ ratios of Figure 24 give the energy absorption buildup factor B_a at the surface of the medium as a function of the distance from the source parallel to the centerline of the void in centimeters and in terms of the mean free path of the uncollided photons in the medium.

The energy absorption buildup factor is defined as

$$B_a = \frac{{}_oD}{{}^o_oD} = \frac{\int_\lambda \mu_a(\lambda)\, I_o(r,\lambda)\, d\lambda}{\mu_a(\lambda_o)\, I_o^o(r, \lambda_o)} \quad .$$

That is, B_a was computed by dividing, at the same distance from the source, the values for the rate at which energy is absorbed at the surface due to photons of all energies by the rate at which energy is absorbed at the surface due to the uncollided surface flux. These values were obtained from Figures 15, 18, 20 and 22. The R = 0 curve of Figure 24 was obtained by dividing, at the same distance from the source, the rate at which energy is absorbed due to photons of all energies by the rate at which energy is absorbed due to the uncollided flux in an infinite medium. Values for this curve were obtained from Figure 12.

Figure 24. Energy absorption buildup factor at the interface as a function of distance along centerline

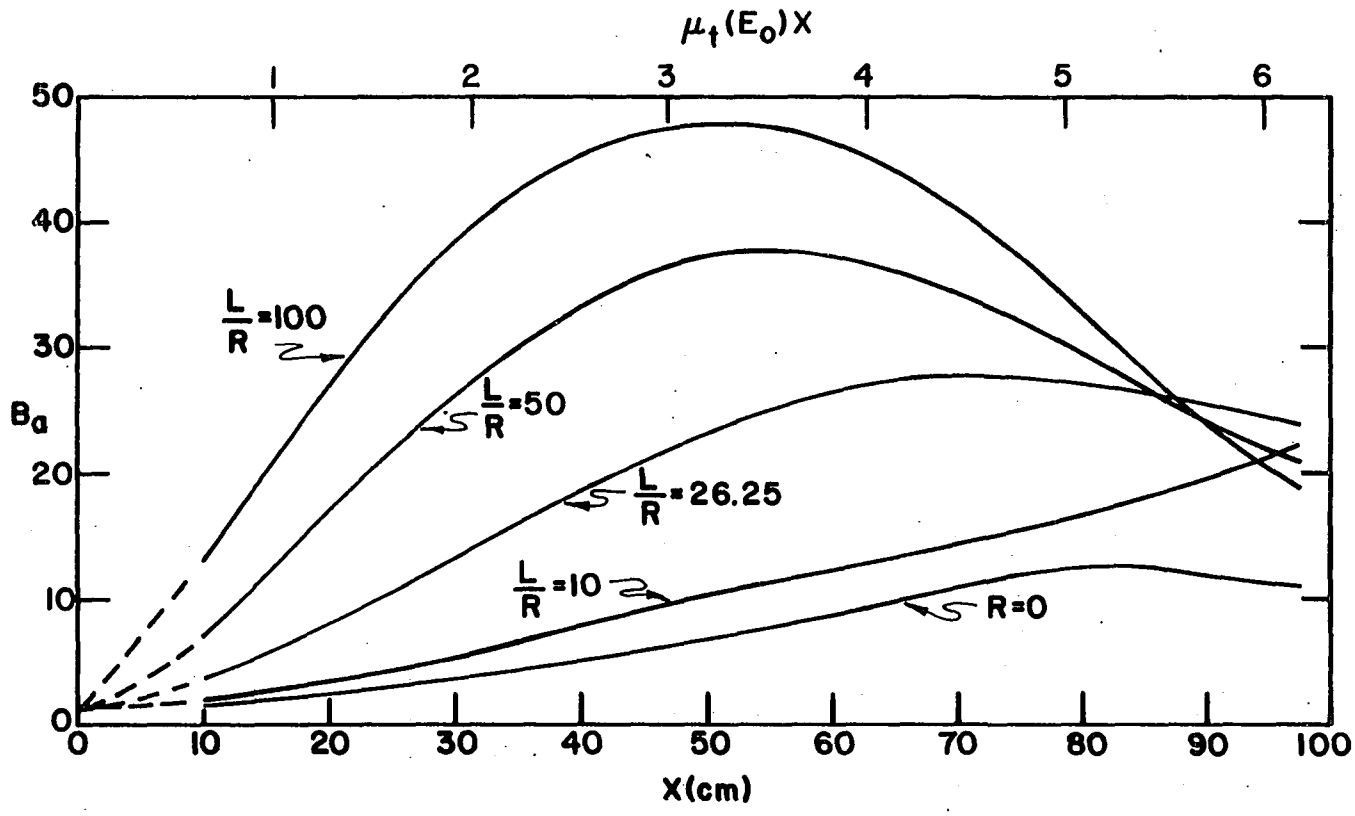
$\mu_t(E_0)X$
1
2
3
4
5
6
50
40
30
20
10
0
B_a
$\frac{L}{R}$=100
$\frac{L}{R}$=50
$\frac{L}{R}$=26.25
$\frac{L}{R}$=10
R=0
0
10
20
30
40
50
60
70
80
90
100
X(cm)

It should be noted that the curves of B_a for the various L/R ratios and the curve of B_a for R = 0 of Figure 24 are fundamentally different. The curves for the various L/R ratios relate the rate of energy absorbed at the medium-void interface to the uncollided photon flux at this surface whereas the R = 0 curve gives B_a for a homogeneous medium. The curve for R = 0 was added to Figure 24 to serve as a reference.

R = 0

From Figure 12 one sees that the rate due to the uncollided flux and the total rate for R = 0 have about the same shape, with the uncollided flux rate having a slightly greater slope. Thus, except for the last 15 cm, where the total rate decreases due to end losses, B_a increases with x.

$L/R \longrightarrow \infty$

As $R \longrightarrow 0$ the curve of the total rate must approach the R = 0 curve. However, one sees from Figure 25 that for small R the curve of the rate due to the uncollided flux at the surface of the void does not approach the rate due to the uncollided flux with no-void. In fact, if the rate due to the uncollided flux at the surface of a small void at x = 100 cm were equal to the rate due to the uncollided flux with no-void at x = 100 cm, then the rate due to the uncollided flux at the surface of the void at x = 50 cm would be less than 10 percent of the rate due to the uncollided flux with no-void at x = 50 cm. Thus at x = 50 cm, B_a would be more than ten times greater for this small void case than for the no-void case.

For example, one can estimate from Figure 25 that the rate due to the

Figure 25. Energy absorption rate at interface due to uncollided flux as a function of distance along centerline

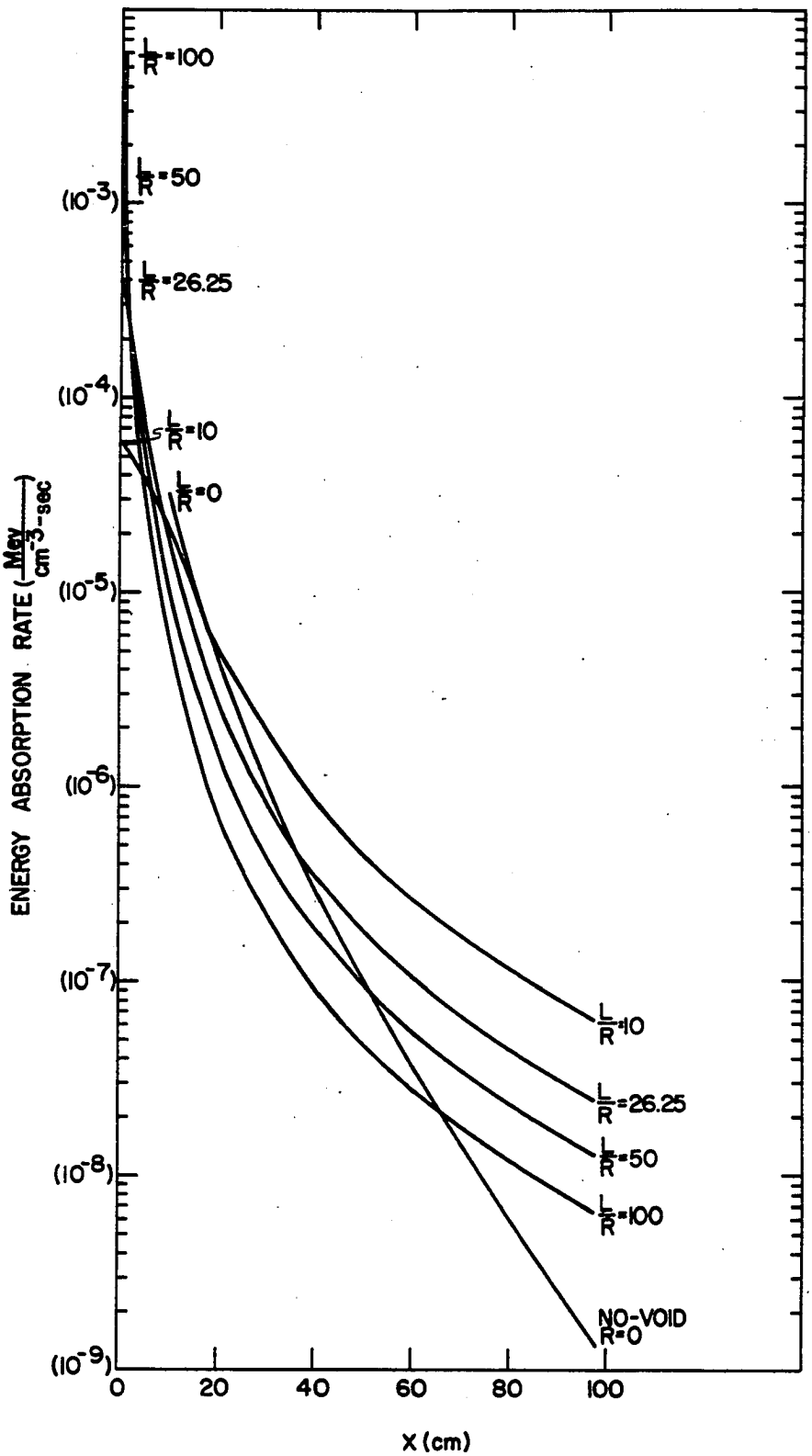
ENERGY ABSORPTION RATE ($\frac{Mev}{cm^3-sec}$)
(10^{-3})
(10^{-4})
(10^{-5})
(10^{-6})
(10^{-7})
(10^{-8})
(10^{-9})
$\frac{L}{R}$=100
$\frac{L}{R}$=50
$\frac{L}{R}$=26.25
$\frac{L}{R}$=10
$\frac{L}{R}$=0
$\frac{L}{R}$=10
$\frac{L}{R}$=26.25
$\frac{L}{R}$=50
$\frac{L}{R}$=100
NO-VOID
R=0
0
20
40
60
80
100
X (cm)

uncollided flux for $L/R \simeq 500$, x = 100 cm is about equal to the rate due to the uncollided flux with no-void at x = 100 cm. From Figure 26 one observes that the total rate at the surface of the void would be approximately the same as if no void existed, i.e. R = 0 case. Thus at x = 100 cm, since the rate due to the uncollided flux for $L/R \simeq 500$ and R = 0 are approximately equal and the total rates for $L/R \simeq 500$ and L/R = 0 are approximately equal, B_a at x = 100 cm for $L/R \simeq 500$ will be approximately equal to B_a at x = 100 cm for R = 0. That is about 11.

At x = 50 cm the rate due to the uncollided flux for $L/R \simeq 500$ will be less than 10 percent of the rate due to the uncollided flux for R = 0, whereas the total rate at x = 50 cm in both cases will be approximately the same. Thus B_a at x = 50 cm for $L/R \simeq 500$ will be greater than 10 times B_a at x = 50 cm for R = 0 which is about 7. That is B_a at x = 50 cm for $L/R \simeq 500$ will be greater than 70.

Of course, for L/R > 500 the rate due to the uncollided surface flux at x = 100 cm will be less than for the no-void case and thus B_a at x = 100 cm for L/R > 500 will exceed B_a at x = 100 cm for R = 0. As $L/R \rightarrow \infty$ the rate due to the uncollided surface flux will approach 0 at all x, while the total rate will approach the R = 0 value, B_a will therefore approach ∞ for all x.

L/R = 100

From Figure 25 one notes that for x > 50 cm the slopes of the curves of the rate due to the uncollided surface flux as a function of x are approximately the same for all L/R. Also from Figure 26 one sees that the slope of the total rate curve for L/R = 100 is only slightly less

Figure 26. Energy absorption rate at interface as a function of distance along centerline

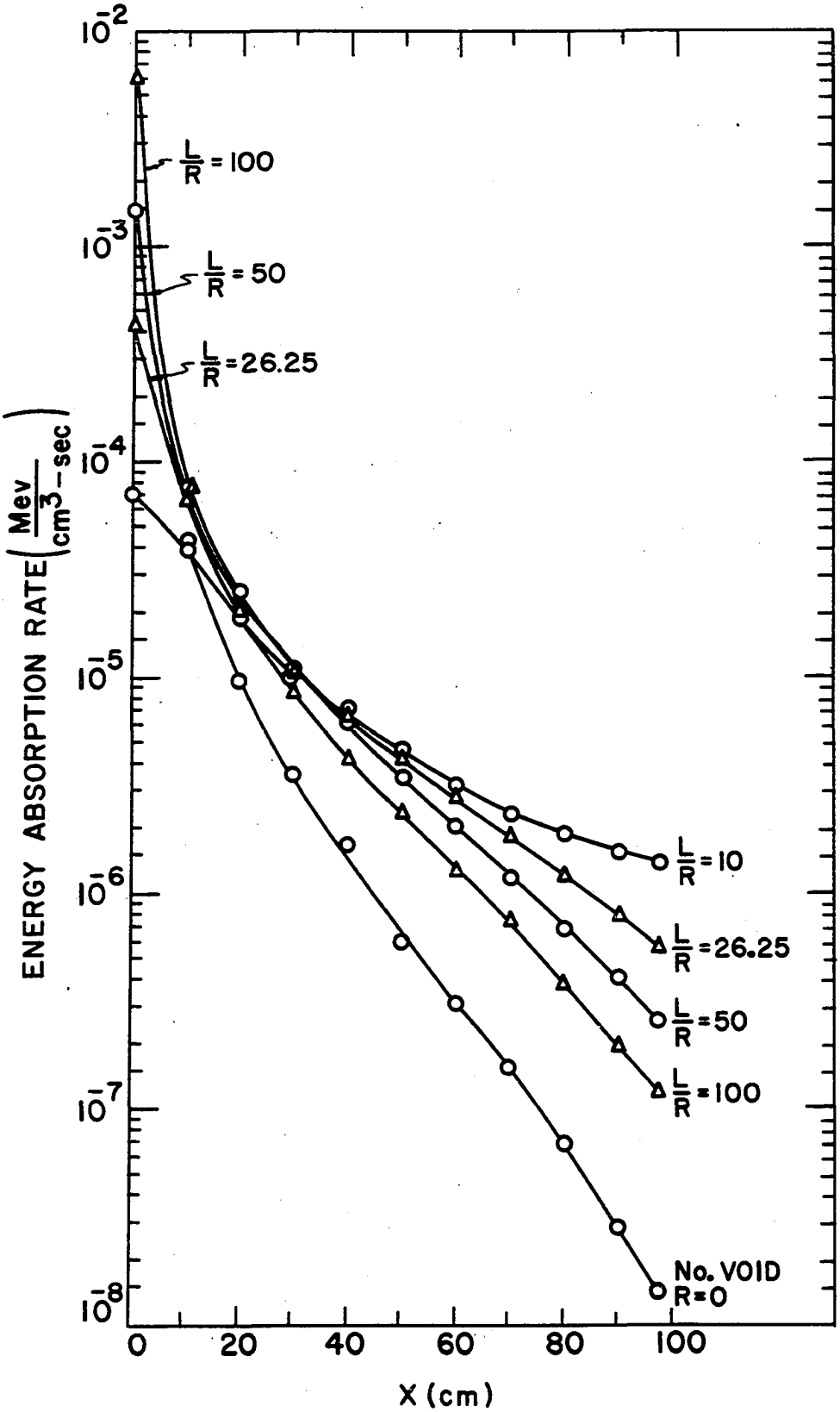
ENERGY ABSORPTION RATE $\left(\frac{\text{Mev}}{\text{cm}^3\text{-sec}}\right)$
10^{-2}
10^{-3}
10^{-4}
10^{-5}
10^{-6}
10^{-7}
10^{-8}
$\frac{L}{R}$ = 100
$\frac{L}{R}$ = 50
$\frac{L}{R}$ = 26.25
$\frac{L}{R}$ = 10
$\frac{L}{R}$ = 26.25
$\frac{L}{R}$ = 50
$\frac{L}{R}$ = 100
No. VOID
R = 0
0
20
40
60
80
100
X (cm)

than, and the shape is approximately the same as, the total rate curve for R = 0. Therefore B_a for L/R = 100 must have approximately the same shape as B_a for L/R = 500, that is a higher value for x = 50 cm than for x = 97.5 cm. However, since there is a slight decrease in the slope of the total rate curve as one goes from R = 0 to L/R = 100 compared to a negligible decrease in the slope of the rate due to the uncollided surface flux as one goes from L/R = 500 to L/R = 100, one would expect the maximum at x 50 cm and the local minimum at x = 97.5 cm of B_a to be less pronounced for L/R = 100 than L/R = 500. That is at x ≃ 50 cm B_a for L/R = 100 should be less than 70 and at x = 97.5 cm it should be greater than 11 which agrees with the curve for B_a as a function of x for L/R = 100 as shown in Figure 24.

L/R = 50 and L/R = 26.25

As L/R decreases from 100 to about 25 the ratio of the maximum value of B_a in the middle range of x to the local minimum value at high x will continue to decrease since the slopes of the total rate curves over this range of x continues to decrease as L/R decreases whereas the slopes of the rate due to the uncollided surface flux curves over this range of x remain essentially constant. The curves for L/R = 50 and L/R = 26.25 in Figure 24 show this trend.

L/R = 10

Between L/R of 25 and L/R = 10 the slope of the total rate curves decreases until, at all values of x, the slope of total rate at a given L/R becomes less than the slope of the rate due to the uncollided surface flux curve at the same value of $\frac{L}{R}$. Thus B_a will be a

continuously increasing function of x. The curve for L/R = 10 in Figure 24 is an example of the continuously increasing B_a as a function of x for low L/R ratios.

L/R < 10

As L/R decreases below 10, both the rate due to the uncollided surface flux and the total rate at the surface will tend to be slowly decreasing functions of x, however the total rate curve at any value of x will always have a slightly smaller slope than the curve for the rate due to the uncollided surface flux at the same value of x. This is because as x increases, the angle of incidence between the uncollided photon and the surface decreases, and as the incident angle of the photon decreases from 90° the probability of absorbing the photons energy near the surface increases. This is merely another way of stating that for L/R < 10 B_a will be a continuously increasing function of x.

In the limiting case, as L/R $\rightarrow$ 0, (assuming that R is still less than ∞ so that some uncollided flux will reach the surface) B_a as a function x will approach a constant since the angle of incidence between the uncollided photons and the surface will approach 90° for all values of x.

Summary

One might expect that whenever the angle between the incident photon and the surface is less at point a than at point b, the buildup factor would be greater at point a than at point b. This, however, is not the case except for voids with small L/R ratios. As is seen in Figure 24, B_a as a function of x for L/R = 100 shows a sharp decrease for x greater

than 60 cm while, of course, the incident angle between the photons and the surface decreases as x increases. The explanation for this apparent discrepancy can be obtained by referring to Figures 25 and 26.

As $L/R \rightarrow \infty$ the uncollided surface flux approaches zero but the energy absorbed at the surface approaches the value of the no-void case. This means that for very large L/R ratios, it is not the uncollided surface flux that determines the energy absorbed at the surface but rather it is the uncollided flux that reaches the vicinity of the surface by traveling through the medium.

This point is demonstrated further in Figure 27. In this Figure a hypothetical buildup factor, B_a', is presented where B_a' is the ratio of the energy that is absorbed at the surface of the void to the energy that is absorbed due to the uncollided flux along the x-axis for the no-void case. That is it compares the total rate curves in Figure 26 to R = 0 curve in Figure 25.

If, as L/R increases, the energy absorbed at the surface becomes increasingly more dependent on the uncollided flux in the vicinity of the void rather than on the uncollided surface flux, then as L/R increases, B_a' at any x should approach B_a' for R = 0. This is the trend that is shown in Figure 27. In the limit, as $L/R \rightarrow \infty$, the energy absorbed at the surface must be completely dependent on the uncollided flux in the vicinity of, rather than at the surface of, the void since the latter goes to zero as $L/R \rightarrow \infty$. Therefore B_a' for $L/R \rightarrow \infty$ becomes identical with B_a' for R = 0.

For L/R = 100, B_a is computed by comparing the total rate at the

Figure 27. Energy absorption buildup factor at interface based on uncollided flux in infinite medium as a

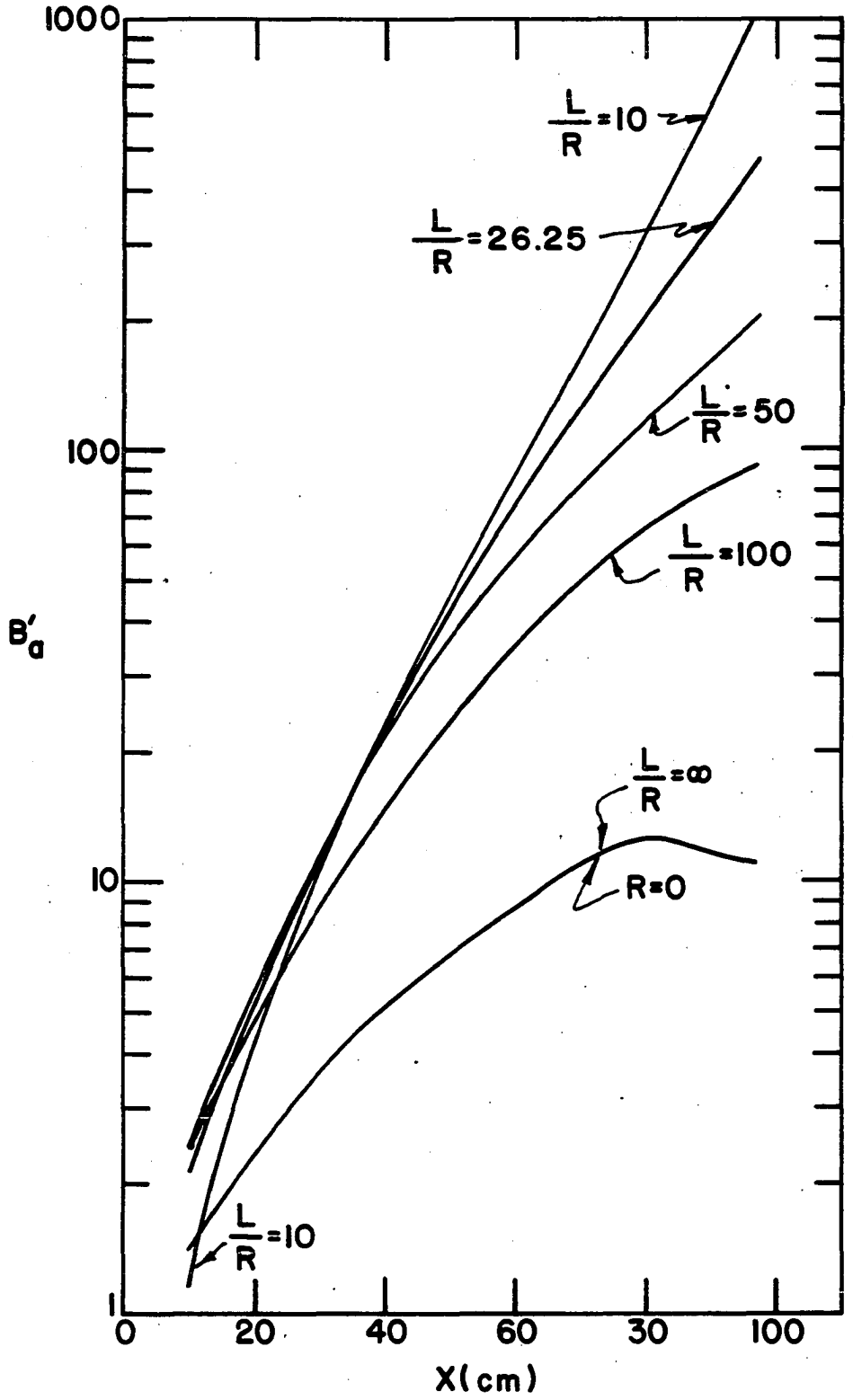
1000
100
10
1
B'_a
$\frac{L}{R}=10$
$\frac{L}{R}=26.25$
$\frac{L}{R}=50$
$\frac{L}{R}=100$
$\frac{L}{R}=\infty$
R=0
$\frac{L}{R}=10$
0
20
40
60
30
100
X(cm)

surface, which is primarily dependent upon and therefore has the approximate shape of the R = 0 curve of Figure 26, to the rate of energy absorbed at the surface due to the uncollided flux, which is the L/R = 100 curve of Figure 25. It must therefore exhibit a maximum somewhere between 30 cm < x < 80 cm and a minimum at x = 97.5 cm.

At the other extreme, that is as $L/R \rightarrow 0$, the rate at which energy is absorbed at the surface is determined almost exclusively by the uncollided surface flux. The total rate curve must therefore follow the curve for the rate at which energy is absorbed due to the uncollided surface flux.

It is for values of $L/R \lesssim 10$ then, where the energy absorbed at the surface is largely determined by the uncollided surface flux, for which one can reason that since the angle of incidence between the uncollided photons and the surface decreases as x increases, B_a must be a continuously increasing function of x.

SUMMARY, CONCLUSIONS AND RECOMMENDATIONS

Summary

The problem of the rate at which energy is absorbed in a shield at the interface between the shield and a cylindrical void through the shield is not amendable to solution by the various semi-analytical methods, e.g. method of moments, successive scattering etc., normally used for determining the flux in infinite media or at locations far distant from a boundary. The Monte Carlo method, on the other hand, is inefficient if one wishes to determine the flux at a great number of positions in a large volume. This method has the flexibility, however, which facilitates the determination of the rate at which energy is absorbed near a boundary by allowing position to be specified by two coordinates.

This investigation utilized the flexibility of the Monte Carlo method by specifying distance along the centerline of the duct x, and radially from the centerline r. The additional variable, r, added considerable complexity to the program but allowed the positioning of the initial collisions near the boundary and the rate at which energy is absorbed to be obtained as a function of distance from the boundary.

Thus, by making use of the flexibility of the Monte Carlo method the maximum concentration of information was obtained at the location under investigation--the boundary. The rate of energy absorbed for each diameter duct at the boundary between the water and the 100 cm long duct was obtained, with a possible 10 percent error, using only 22,000

histories or approximately 3.5 hours of time on the IBM 7074 computer per run.

Conclusions

1. The problem of determining the rate at which energy is absorbed, at the interface between a water shield and a cylinderical void through the shield, due to an isotropic point source of cobalt-60 located on the centerline of the void was successfully attacked by means of Monte Carlo calculations.

2. The rate at which energy is absorbed at the interface of the voids with $\frac{L}{R}$ ratios less than 10 is dependent primarily upon the uncollided surface flux at the interface.

3. The rate at which energy is absorbed at the interface of the voids with $\frac{L}{R}$ ratios greater than 50 is dependent primarily upon the uncollided flux in the medium near the void.

4. The influence of the void on the rate at which energy is absorbed at the interface between the void and the shield is more pronounced a) as the size of the void increases and b) as distance from the source increases.

5. The energy absorption buildup factor at the interface of the void with an $\frac{L}{R}$ ratio less than 10 is a continuously increasing function of the distance from the source along the centerline of the void.

6. The energy absorption buildup factor at the interface of the voids with $\frac{L}{R}$ ratios greater than 50 exhibits a maximum between 20 cm and 80 cm from the source.

Recommendations

The present investigation could be extended to obtain the rate of energy absorbed at the shield duct interface due to a plane source rather than a point source by modifying only that part of the program concerned with the weight of the photon due to the position of its initial collision. This change would further complicate the program but would not require an appreciable addition in computer time to obtain the same accuracy of data.

An ambitious extension of the method of positioning the first collision might be to specify the position of the second scattering collision and then calculate the appropriate weight factors for these positions. This would be somewhat like combining the method of successive scattering and the Monte Carlo method. Since the energy of the source photons is known it would be possible, in principle, to calculate the distribution of position and energy at which the photons undergo their second collision. From this the weight factors for the photons could be calculated and the succeeding histories of the photons determined by the Monte Carlo method. This combination method would reduce computer time at the expense of increasing the complexity of the program and should possibly be considered for boundary problems that require a great deal of computer time by the Monte Carlo method.

A more extensive application of the techniques of dimensional analysis to the problems of gamma shielding should prove fruitful. It is possible that this tool could prove to be as useful in the field of nuclear engineering as it has been in the fields of heat transfer and fluid mechanics.

LITERATURE CITED

1. Foldy, L. L. Physics Reviews 81: 395 (1951); 81: 400 (1951).

2. Bethe, H. A., Fano, U., and Karr, P. R. Physics Reviews 76: 538 1949.

3. Wilkins, J. E., Jr., Oppenheim, A., and Solon, L. U.S. Atomic Energy Commission Report NYO-633 [New York Operations Office, AEC]. 1950.

4. Welton, T. A. U.S. Atomic Energy Commission Report TID-256 [Technical Information Service Extension, AEC]. 1955.

5. Solon, L. R. and Wilkins, J. E., Jr. U.S. Atomic Energy Commission Report NYO-635 [New York Operations Office, AEC]. 1950.

6. Solon, L. R., Wilkins, J. E., Jr., Oppenheim, A., and Goldstein, H. U.S. Atomic Energy Commission Report NYO-637 [New York Operations Office, AEC]. 1951.

7. Goldstein, H. Fundamental aspects of reactor shielding. Reading, Mass., Addison-Wesley Publishing Co., Inc. 1958.

8. Cave, L., Corner, J., and Liston, R.H.A. Royal Society Proceedings Series A, 204: 223. 1950.

9. Peebles, G. H. and Plesset, M. S. U.S. Atomic Energy Commission Report P-88 [Rand Corp., Santa Monica, Calif.]. 1950.

10. Peebles, G. H. and Plesset, M. S. Physics Reviews 81: 430. 1951.

11. Peebles, G. H. Journal of Applied Physics 24: 1272 and 1437. 1953.

12. Spencer, L. V. and Fano, U. Physics Reviews 81: 464. 1951.

13. Spencer, L. V. and Fano, U. National Bureau of Standards Journal of Research 46: 446. 1951.

14. Fano, U., Spencer, L. V., and Berger, M. J. Encyclopedia of Physics 38, Part 2: 660. 1959.

15. Wick, G. C. Physics Reviews 75: 738. 1949.

16. Fano, U. National Bureau of Standards Journal of Research 51: 95. 1953.

17. Spencer, L. V. Physics Reviews 88: 793. 1952.

18. Theus, R. B. and Beach, L. A. Washington D.C., Naval Research Laboratory Quarterly on Nuclear Science and Technology, July - September 1953.

19. Rockwell, T., III. Reactor shielding design manual. Princeton, New Jersey, D. Van Nostrand Company, Inc. 1956.

20. Price, B. T., Horton, C. C., and Spinney, K. T. Radiation shielding. New York, N.Y., Pergamen Press. 1957.

21. Kahn, H. Nucleonics, 6, No. 5: 27 (1950); and 6, No. 6: 50 (1950).

22. Kahn, H. U. S. Atomic Energy Commission Report P-88 [Rand Corp., Santa Monica, Calif.]. 1949.

23. Collins, D. G. American Nuclear Society Transactions 5: 396. 1962.

24. Goldstein, H. and Wilkins, J. E., Jr. U.S. Atomic Energy Commission Report NYO 3075 [New York Operations Office, AEC]. 1954.

25. Grodstein, G. W. National Bureau of Standard, Circular 583. 1959.

26. Goldstein, H. The attenuation of gamma rays and neutrons in reactor shields. Washington D.C., U.S. Government Printing Office. 1957.

27. Kays, J. C. Gamma field in water surrounding a duct containing a source. Unpublished M.S. thesis. Ames, Iowa, Library, Iowa State University of Science and Technology. 1963.

28. Murphy, G. Similitude in engineering. New York, N.Y., The Ronald Press Company. 1950.

ACKNOWLEDGEMENTS

The author wishes to acknowledge his sincere gratitude to Dr. Glenn Murphy, Head of the Department of Nuclear Engineering, for his many helpful suggestions, continued support and encouragement throughout the investigation; and to Dr. Willard H. McCorkle, Chief of the Reactor Division of the United States Atomic Energy Commission, Ames Laboratory for making the necessary computer time available.

Recognition is also extended to Dr. Herbert T. David of the Statistics Department and to Mr. William J. Higby and Mr. David E. Erbeck of the Ames Laboratory for their invaluable help in the computer programming.

The deepest appreciation is expressed to the author's wife, Ruth, for her aid, encouragement, unending patience and moral support during the course of this investigation.

APPENDIX A

First Collision Weight Factor

Figure 28 gives the geometry used to determine the first collision weight factor.

$$\left(\begin{array}{l}\text{The probability of}\\ \text{the first collision}\\ \text{occurring at } \vec{r}_1\\ \text{where } |\vec{r}_i| = \xi_1\end{array}\right) = \left(\begin{array}{l}\text{Probability that the}\\ \text{angle } \omega_1 \text{ is subtonded}\\ \text{by a ring of area dA}\\ \text{at } \vec{r}_1 \text{ on the surface of}\\ \text{a sphere of radius } \xi_1\end{array}\right) \times$$

$$\left(\begin{array}{l}\text{Probability of traveling}\\ \text{through water a distance}\\ \text{equal to } (\xi_1)_m\end{array}\right) \times$$

$$\left(\begin{array}{l}\text{Volume incompsins}\\ \vec{r}_1\end{array}\right) \times$$

$$\left(\begin{array}{l}\text{Probability of not}\\ \text{leaving shield by}\\ \text{passage through}\\ \text{void alone}\end{array}\right) \times$$

$$\left(\text{Normalizing constant}\right)$$

or

$$W_1 = P_{\omega_1} \; P_{(\xi_1)_m} \; V_1 \; P_{v_1} N_1$$

where

Figure 28. Geometry for first collision weight factor

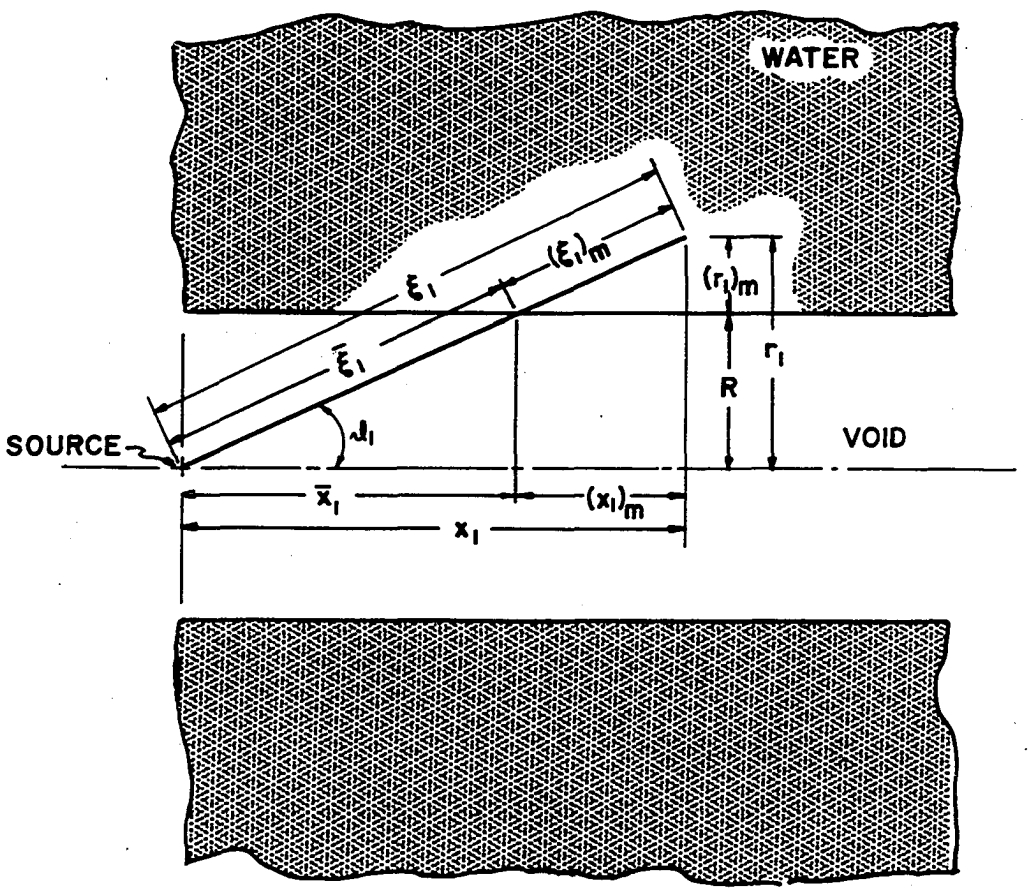
WATER
ξ_1
$(\xi_1)_m$
$(r_1)_m$
$\bar{\xi}_1$
r_1
R
SOURCE
α_1
VOID
$\bar{x}_1$
$(x_1)_m$
x_1

P_{ω_1}

The probability that the angle ω_1 is subtended by a ring of unit area at $\vec{r}_1$ on the surface of a sphere of radius ξ_1 is

$$P_{\omega_1} = \frac{1}{4\pi\,(\xi_1)^2} = \frac{1}{4\pi\,(x_1^2 + r_1^2)}$$

$P_{(\xi_1)_m}$

The porbability of traveling through water a distance equal to $(\xi_1)_m$ is

$$P_{(\xi_1)_m} = \mu_1 e^{-\mu_1(\xi_1)_m}$$

or

$$\mu_1 e^{-\frac{\mu_1(r_1-R)}{\sin_1}}$$

or

$$P_{(\xi_1)_m} = \mu_1 e^{-\frac{\mu_1(r_1-R)(x_1^2 + r_1^2)^{\frac{1}{2}}}{r_1}}$$

V_1 = the volume of shield encompsing $\vec{r}_1$ is

$$V_1 = \pi \left[(r_1 + \tfrac{\Delta r}{2})^2 - (r_1 - \tfrac{\Delta r}{2})^2 \right] \Delta x_v$$

P_{v_1}

Figure 29 gives a sketch of the geometry used in determining the probability of the proton not leaving the shield by passage through void alone.

The area on the surface of the sphere of radius ρ subtending the angle $d\psi'$ at ψ' is

$$(2\pi\rho \sin \psi')(\rho\, d\psi')$$

Figure 29. Geometry for passage through void

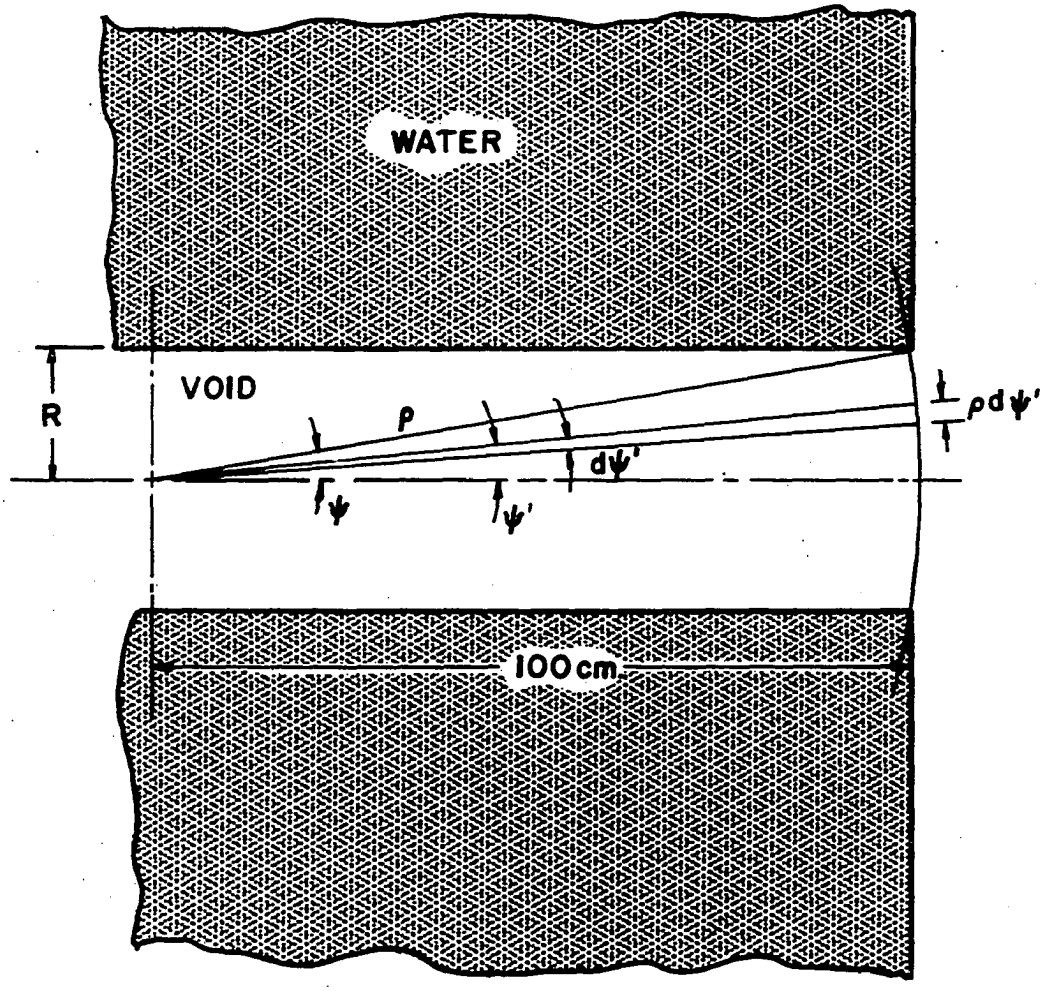
WATER
VOID
R
ρ
dψ'
ρdψ'
ψ
ψ'
100 cm

thus

$$P_v = 1 - \frac{\int_o^{\psi} 2\pi \rho^2 \sin \psi' \, d\psi'}{2\pi\rho^2}$$

$$P_v = 1 + \cos \psi' - 1$$

or

$$P_v = \cos \left(\tan^{-1} \frac{R}{100}\right)$$

$\underline{N_1}$

In order for the sum of the first collision weights for all positions of first collisions to equal unity the normalizing constant must be

$$N_1 = \frac{1}{\sum_{k=o}^{10} \sum_{j=o}^{9} {}_k(P_{\vartheta_1})_i^j \; {}_k(P_{(\xi_1)_m})_i^j \; {}_k(V_1)_i^j \; (P_{v_1})_i}$$

APPENDIX B

Change in Position

Figure 30 gives the geometry used in determining the change in position. Consider three cases.

1. If $r_n \sin \phi_{n+1} > R$

Then Distance photon travels through material = Distance between n-th and the (n+1)st collision

$$(\xi_n)_m = \xi_n$$

2. If a) $r_n \sin \phi_{n+1} < R$

and b) $\xi_n < \dfrac{r_n \cos \phi_{n+1} - [R^2 - r_n^2 \sin^2 \phi_{n+1}]^{\frac{1}{2}}}{\sin \theta_{n+1}}$

Then

$$(\xi_n)_m = \xi_n$$

3. If a) $r_n \sin \phi_{n+1} < R$

and b) $\xi_n > \dfrac{r_n \cos \phi_{n+1} - [R^2 - r_n^2 \sin^2 \phi_{n+1}]}{\sin \theta_{n+1}}$

Then distance photon travels through material + distance photon travels through void = distance from n-th to (n+1) st collision

$$(\xi_n)_m + \bar{\xi}_n = \xi_n$$

or

$$(\xi_n)_m + \frac{2\,[R^2 - r_n^2 \sin^2 \phi_{n+1}]^{\frac{1}{2}}}{\sin \theta_{n+1}} = \xi_n$$

The general distribution function for the distance between collisions will be

$$f(\xi_n) = \mu\,(\lambda_{n+1})_e^{-\mu(\lambda_{n+1})\xi_n}$$

For case (1) and (2) (i.e. photon not entering void)

$$f(\xi_n) = \mu\,(\lambda_{n+1})\, e^{-\mu(\lambda_{n+1})\xi_n}$$

Figure 30. Geometry for change in position

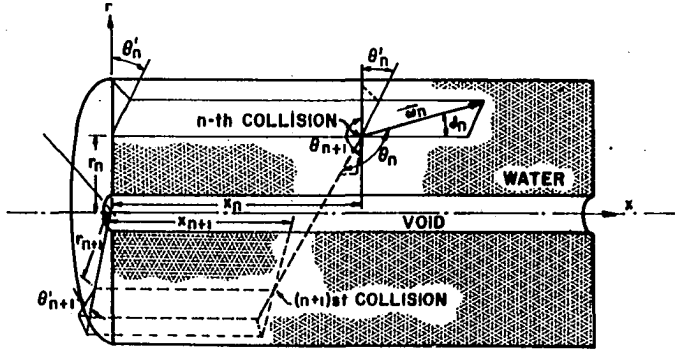

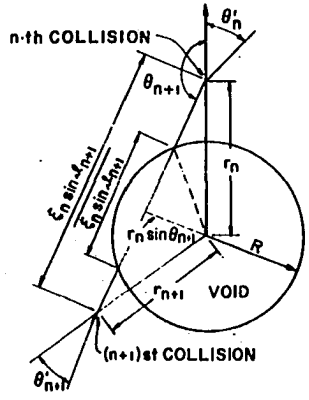

END VIEW

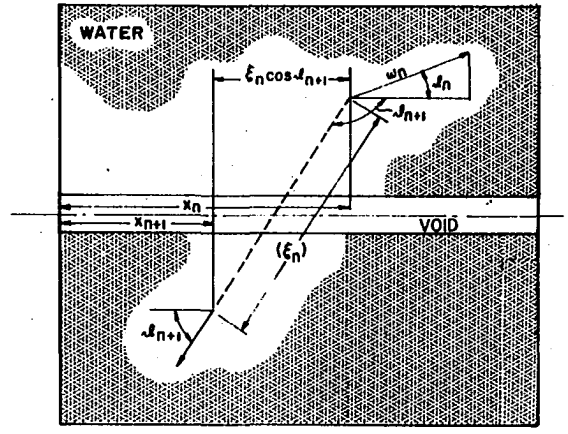

SIDE VIEW

and

$$x_{n+1} = x_n + \xi_n \cos \vartheta_{n+1}$$

$$r_{n+1} = \sqrt{r_n^2 + (\xi_n \sin \vartheta_{n+1})^2 - 2 r_n \xi_n \sin \vartheta_{n+1} \cos \phi_{n+1}}$$

But for (3) (through void)

$$f[(\xi_n)_m] = \mu(\lambda_{n+1}) e^{-\mu(\lambda_{n+1})(\xi_n)_m}$$

where

$$\xi_n = \bar{\xi}_n + (\xi_n)_m \qquad \begin{cases} \bar{\xi}_n = \text{distance through void} \\ (\xi_n)_m = \text{distance through material} \end{cases}$$

and

$$x_{n+1} = x_n + \xi_n \cos \vartheta_{n+1}$$

$$r_{n+1} = \sqrt{r_n^2 + (\xi_n \sin \vartheta_{n+1})^2 - 2 r_n \xi_n \sin \vartheta_{n+1} \cos \phi_{n+1}}$$

where

$$\xi_n = \frac{2[R^2 - r_n^2 \sin^2 \phi_{n+1}]^{\frac{1}{2}}}{\sin \vartheta_{n+1}} + (\xi_n)_m$$

For the cumulative distribution

$$F[(\xi_n)_m] = \mu(\lambda_{n+1}) \int_{\xi_n}^{\infty} e^{-\mu(\lambda_{n+1})\xi'} d\xi'$$

the selection rule is

$$(\xi_n)_m = -\frac{1}{\mu(\lambda_{n+1})} \log q \qquad q \text{ random on } (0,1).$$

From the law of cosines ϕ'_{n+1} is given by

$$\cos \phi'_{n+1} = \frac{r_{n+1}^2 - r_n^2 + (\xi_n \sin \vartheta_{n+1})^2}{2 r_{n+1} (\xi_n \sin \vartheta_{n+1})}$$

APPENDIX C

Uncollided Flux at Surface of Void

The fraction of the source photons that cross the surface dS at R and x (Figure 31) is

$$\frac{dS}{2\pi r^2} = \frac{2\pi R \sin\theta \, dx}{2\pi r^2}$$

but

$$r = \frac{R}{\sin \theta}$$

therefore

$$\frac{dS}{2\pi r^2} = \frac{\sin^3 \theta \, dx}{R} .$$

The number of photons that cross the surface per second from a point isotropic source of cobalt-60 that is on the centerline of the void at x = o and that has a strength of 1 disintegration per second (i.e. two photons per second) is

$$\frac{(1) \sin^3 \theta \, dx}{R} .$$

Thus the uncollided photon number current (i.e. the number of photons per unit area that cross the surface per unit time) is given by

$$\frac{\sin^3 \theta \, dx}{R \, (2\pi \, R \, dx)}$$

or

$$\frac{\sin^3 \theta}{2\pi R^2} .$$

However the uncollided photon number current, in a void, is equal to the uncollided photon number flux. That is

Figure 31. Geometry for uncollided surface flux

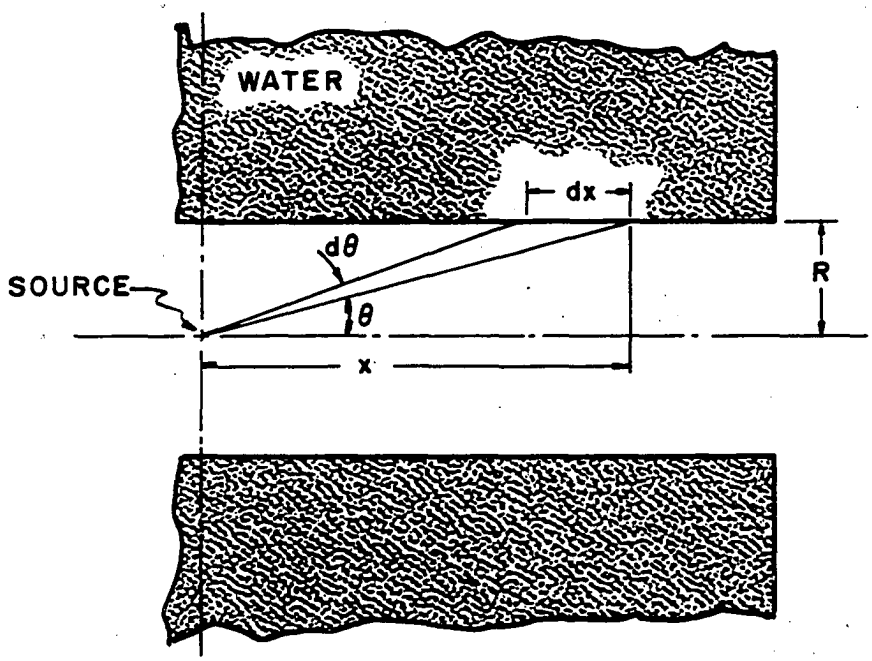
WATER
dx
dθ
SOURCE
θ
R
x

$$N_o^o = \frac{\sin^3 \theta}{2\pi R^2} \quad .$$

The uncollided photon energy flux, I_o^o, is

$$I_o^o = E_o N_o \quad \text{Mev/cm}^2\text{-sec}$$

that is

$$I_o^o = \frac{E_o \sin^3 \theta}{2\pi R^2} \qquad \text{Mev/cm}^2\text{-sec}$$

The energy absorption coefficient, $\mu_a (\lambda_o)$, is defined by

$$\mu_a (\lambda_o) = \frac{\bar{E}}{E_o} \mu_t (\lambda_o) \text{ cm}^{-1}$$

where $\mu_t (\lambda_o)$ = total absorption coefficient

and $\frac{\bar{E}}{E_o}$ = the average fraction of the energy transfored by the photon (of energy E_o) to the medium on each collision

Therefore the rate at which energy is absorbed at the surface of the void is $\mu_a (\lambda_o) I_o^o$

where

$$\mu_a (\lambda_o) I_o^o = \frac{\mu_o(\lambda_o) E_o \sin^3 \theta}{2\pi R^2} \qquad \text{Mev/cm}^3\text{-sec}$$

or

$$\mu_a (\lambda_o) I_o^o = \frac{\mu_a (\lambda_o) E_o \sin^3 (\tan^{-1} \frac{R}{x})}{2 \pi R^2} \quad \text{Mev/cm}^3\text{-sec}$$

APPENDIX D

Table 3. Energy absorption rate (Mev/cm^3-sec) Run 09-23-63 R = 0 cm

Horiz. Dist. From Source (cm)	0.000	1.000	2.000	3.000	4.000	Radial 5
0.0	0.143 (10^{-1})	0.178 (10^{-2})	0.630 (10^{-3})	0.372 (10^{-3})	0.214 (10^{-3})	0.1
5.0	0.462 (10^{-4})	0.449 (10^{-4})	0.384 (10^{-4})	0.349 (10^{-4})	0.286 (10^{-4})	0.1
15.0	0.102 (10^{-4})	0.917 (10^{-5})	0.105 (10^{-5})	0.106 (10^{-4})	0.846 (10^{-5})	0.6
25.0	0.384 (10^{-5})	0.672 (10^{-5})	0.402 (10^{-5})	0.318 (10^{-5})	0.316 (10^{-5})	0.2
35.0	0.134 (10^{-5})	0.131 (10^{-5})	0.218 (10^{-5})	0.251 (10^{-5})	0.159 (10^{-5})	0.1
45.0	0.180 (10^{-5})	0.669 (10^{-6})	0.534 (10^{-6})	0.660 (10^{-6})	0.533 (10^{-6})	0.5
55.0	0.316 (10^{-6})	0.338 (10^{-6})	0.327 (10^{-6})	0.292 (10^{-6})	0.418 (10^{-6})	0.3
65.0	0.110 (10^{-6})	0.176 (10^{-6})	0.226 (10^{-6})	0.128 (10^{-6})	0.163 (10^{-6})	0.1
75.0	0.762 (10^{-7})	0.194 (10^{-6})	0.715 (10^{-7})	0.544 (10^{-7})	0.128 (10^{-6})	0.4
85.0	0.281 (10^{-7})	0.434 (10^{-7})	0.366 (10^{-7})	0.263 (10^{-7})	0.178 (10^{-7})	0.2
95.0	0.755 (10^{-8})	0.207 (10^{-7})	0.685 (10^{-8})	0.200 (10^{-7})	0.166 (10^{-7})	0.9

= 0 cm

	Radial Distance					
	4.000	5.000	10.000	15.000	20.000	25.000
10^{-3})	0.214 (10^{-3})	0.103 (10^{-3})	0.348 (10^{-4})	0.154 (10^{-4})	0.793 (10^{-5})	0.471 (10^{-5})
10^{-4})	0.286 (10^{-4})	0.133 (10^{-4})	0.133 (10^{-4})	0.764 (10^{-5})	0.432 (10^{-5})	0.273 (10^{-5})
10^{-4})	0.846 (10^{-5})	0.674 (10^{-5})	0.536 (10^{-5})	0.338 (10^{-5})	0.200 (10^{-5})	0.137 (10^{-5})
10^{-5})	0.316 (10^{-5})	0.217 (10^{-5})	0.178 (10^{-5})	0.141 (10^{-5})	0.103 (10^{-5})	0.588 (10^{-6})
10^{-5})	0.159 (10^{-5})	0.106 (10^{-5})	0.807 (10^{-6})	0.623 (10^{-6})	0.569 (10^{-6})	0.375 (10^{-6})
10^{-6})	0.533 (10^{-6})	0.503 (10^{-6})	0.380 (10^{-6})	0.289 (10^{-6})	0.199 (10^{-6})	0.171 (10^{-6})
10^{-6})	0.418 (10^{-6})	0.350 (10^{-6})	0.214 (10^{-6})	0.108 (10^{-6})	0.104 (10^{-6})	0.889 (10^{-7})
10^{-6})	0.163 (10^{-6})	0.115 (10^{-6})	0.102 (10^{-6})	0.607 (10^{-7})	0.700 (10^{-7})	0.388 (10^{-7})
10^{-7})	0.128 (10^{-6})	0.460 (10^{-7})	0.538 (10^{-7})	0.296 (10^{-7})	0.216 (10^{-7})	0.395 (10^{-7})
10^{-7})	0.178 (10^{-7})	0.211 (10^{-7})	0.273 (10^{-7})	0.130 (10^{-7})	0.141 (10^{-7})	0.859 (10^{-8})
10^{-7})	0.166 (10^{-7})	0.927 (10^{-8})	0.146 (10^{-7})	0.634 (10^{-8})	0.709 (10^{-8})	0.276 (10^{-8})

Table 4. Energy absorption rate (Mev/cm^3-sec) Run 10-21-63, R = 1.00 cm

Horiz. Dist. From Source (cm)	1.000	2.000	3.000	4.000	5.000	Radial Dist
0.0	0.235 (10^{-2})	0.911 (10^{-3})	0.442 (10^{-3})	0.294 (10^{-3})	0.186 (10^{-3})	C
5.0	0.691 (10^{-4})	0.548 (10^{-4})	0.438 (10^{-4})	0.388 (10^{-4})	0.353 (10^{-4})	C
15.0	0.171 (10^{-4})	0.145 (10^{-4})	0.148 (10^{-4})	0.137 (10^{-4})	0.104 (10^{-4})	C
25.0	0.789 (10^{-5})	0.741 (10^{-5})	0.470 (10^{-5})	0.463 (10^{-5})	0.429 (10^{-5})	C
35.0	0.390 (10^{-5})	0.289 (10^{-5})	0.288 (10^{-5})	0.219 (10^{-5})	0.235 (10^{-5})	C
45.0	0.219 (10^{-5})	0.137 (10^{-5})	0.170 (10^{-5})	0.103 (10^{-5})	0.104 (10^{-5})	C
55.0	0.140 (10^{-5})	0.749 (10^{-6})	0.642 (10^{-6})	0.643 (10^{-6})	0.583 (10^{-6})	C
65.0	0.693 (10^{-6})	0.352 (10^{-6})	0.394 (10^{-6})	0.384 (10^{-6})	0.413 (10^{-6})	C
75.0	0.281 (10^{-6})	0.280 (10^{-6})	0.177 (10^{-6})	0.138 (10^{-6})	0.144 (10^{-6})	C
85.0	0.159 (10^{-6})	0.845 (10^{-7})	0.517 (10^{-7})	0.672 (10^{-7})	0.406 (10^{-7})	C
95.0	0.152 (10^{-6})	0.443 (10^{-7})	0.626 (10^{-7})	0.272 (10^{-7})	0.439 (10^{-7})	C

R = 1.00 cm

	Radial Distance					
000	5.000	6.000	11.000	16.000	21.000	26.000
4 (10^{-3})	0.186 (10^{-3})	0.857 (10^{-4})	0.326 (10^{-4})	0.153 (10^{-4})	0.804 (10^{-5})	0.457 (10^{-5})
3 (10^{-4})	0.353 (10^{-4})	0.271 (10^{-4})	0.141 (10^{-4})	0.849 (10^{-5})	0.482 (10^{-5})	0.289 (10^{-5})
7 (10^{-4})	0.104 (10^{-4})	0.903 (10^{-5})	0.623 (10^{-5})	0.387 (10^{-5})	0.257 (10^{-5})	0.159 (10^{-5})
3 (10^{-5})	0.429 (10^{-5})	0.332 (10^{-5})	0.240 (10^{-5})	0.174 (10^{-5})	0.134 (10^{-5})	0.822 (10^{-6})
9 (10^{-5})	0.235 (10^{-5})	0.144 (10^{-5})	0.124 (10^{-5})	0.819 (10^{-6})	0.684 (10^{-6})	0.452 (10^{-6})
3 (10^{-5})	0.104 (10^{-5})	0.734 (10^{-6})	0.571 (10^{-6})	0.449 (10^{-6})	0.325 (10^{-6})	0.239 (10^{-6})
3 (10^{-6})	0.583 (10^{-6})	0.433 (10^{-6})	0.312 (10^{-6})	0.204 (10^{-6})	0.148 (10^{-6})	0.996 (10^{-7})
4 (10^{-6})	0.413 (10^{-6})	0.173 (10^{-6})	0.139 (10^{-6})	0.129 (10^{-6})	0.112 (10^{-6})	0.553 (10^{-7})
8 (10^{-6})	0.144 (10^{-6})	0.110 (10^{-6})	0.861 (10^{-7})	0.505 (10^{-7})	0.335 (10^{-7})	0.373 (10^{-7})
2 (10^{-7})	0.406 (10^{-7})	0.432 (10^{-7})	0.374 (10^{-7})			
2 (10^{-7})	0.439 (10^{-7})	0.222 (10^{-7})	0.196 (10^{-7})			

Table 5. Energy absorption rate (Mev/cm^3-sec), R = 2.00 cm

Horiz. Dist. From Source (cm)	2.000	3.000	4.000	5.000	6.000
0.0	0.963 (10^{-3})	0.513 (10^{-3})	0.302 (10^{-3})	0.216 (10^{-3})	0.145 (10^{-3}
5.0	0.699 (10^{-4})	0.575 (10^{-4})	0.455 (10^{-4})	0.421 (10^{-4})	0.351 (10^{-4}
15.0	0.230 (10^{-4})	0.159 (10^{-4})	0.156 (10^{-4})	0.146 (10^{-4})	0.123 (10^{-4}
25.0	0.106 (10^{-4})	0.755 (10^{-5})	0.655 (10^{-5})	0.554 (10^{-5})	0.536 (10^{-5}
35.0	0.521 (10^{-5})	0.380 (10^{-5})	0.316 (10^{-5})	0.347 (10^{-5})	0.272 (10^{-5}
45.0	0.306 (10^{-5})	0.231 (10^{-5})	0.167 (10^{-5})	0.204 (10^{-5})	0.142 (10^{-5}
55.0	0.201 (10^{-5})	0.126 (10^{-5})	0.101 (10^{-5})	0.857 (10^{-6})	0.731 (10^{-6}
65.0	0.154 (10^{-5})	0.642 (10^{-6})	0.607 (10^{-6})	0.388 (10^{-6})	0.340 (10^{-6}
75.0	0.528 (10^{-6})	0.413 (10^{-6})	0.421 (10^{-6})	0.212 (10^{-6})	0.373 (10^{-6}
85.0	0.390 (10^{-6})	0.192 (10^{-6})	0.142 (10^{-6})	0.112 (10^{-6})	0.884 (10^{-7}
95.0	0.252 (10^{-6})	0.105 (10^{-6})	0.633 (10^{-7})	0.113 (10^{-6})	0.663 (10^{-7}

	Radial Distance From Source					
)00	6.000	7.000	12.000	17.000	22.000	27.000
5 (10^{-3})	0.145 (10^{-3})	0.730 (10^{-4})	0.276 (10^{-4})	0.130 (10^{-4})	0.764 (10^{-5})	0.428 (10^{-5})
L (10^{-4})	0.351 (10^{-4})	0.272 (10^{-4})	0.137 (10^{-4})	0.793 (10^{-5})	0.480 (10^{-5})	0.281 (10^{-5})
5 (10^{-4})	0.123 (10^{-4})	0.974 (10^{-5})	0.632 (10^{-5})	0.405 (10^{-5})	0.272 (10^{-5})	0.170 (10^{-5})
+ (10^{-5})	0.536 (10^{-5})	0.400 (10^{-5})	0.275 (10^{-5})	0.204 (10^{-5})	0.126 (10^{-5})	0.929 (10^{-6})
7 (10^{-5})	0.272 (10^{-5})	0.183 (10^{-5})	0.128 (10^{-5})	0.101 (10^{-5})	0.739 (10^{-6})	0.502 (10^{-6})
+ (10^{-5})	0.142 (10^{-5})	0.100 (10^{-5})	0.595 (10^{-6})	0.529 (10^{-6})	0.389 (10^{-6})	0.274 (10^{-6})
7 (10^{-6})	0.731 (10^{-6})	0.561 (10^{-6})	0.352 (10^{-6})	0.246 (10^{-6})	0.189 (10^{-6})	0.137 (10^{-6})
3 (10^{-6})	0.340 (10^{-6})	0.251 (10^{-6})	0.176 (10^{-6})	0.122 (10^{-6})	0.111 (10^{-6})	0.111 (10^{-6})
2 (10^{-6})	0.373 (10^{-6})	0.137 (10^{-6})	0.944 (10^{-7})	0.693 (10^{-7})	0.527 (10^{-7})	0.492 (10^{-7})
2 (10^{-6})	0.884 (10^{-7})	0.783 (10^{-7})	0.474 (10^{-7})	0.282 (10^{-7})	0.242 (10^{-7})	0.199 (10^{-7})
5 (10^{-6})	0.663 (10^{-7})	0.412 (10^{-7})	0.362 (10^{-7})	0.194 (10^{-7})	0.108 (10^{-7})	0.778 (10^{-8})

Table 6. Energy Absorption rate (Mev/cm^3-sec) Run 10-01-63, R = 3.81 cm

Horiz. Dist. From Source (cm)	3.810	4.810	5.810	6.810	7.810	Ra
0.0	0.355 (10^{-3})	0.240 (10^{-3})	0.172 (10^{-3})	0.128 (10^{-3})	0.998 (10^{-4})	
5.0	0.656 (10^{-4})	0.528 (10^{-4})	0.452 (10^{-4})	0.410 (10^{-4})	0.355 (10^{-4})	
15.0	0.223 (10^{-4})	0.179 (10^{-4})	0.163 (10^{-4})	0.149 (10^{-4})	0.127 (10^{-4})	
25.0	0.997 (10^{-5})	0.917 (10^{-5})	0.751 (10^{-5})	0.665 (10^{-5})	0.609 (10^{-5})	
35.0	0.607 (10^{-5})	0.495 (10^{-5})	0.359 (10^{-5})	0.364 (10^{-5})	0.305 (10^{-5})	
45.0	0.344 (10^{-5})	0.268 (10^{-5})	0.282 (10^{-5})	0.208 (10^{-5})	0.176 (10^{-5})	
55.0	0.257 (10^{-5})	0.240 (10^{-5})	0.129 (10^{-5})	0.113 (10^{-5})	0.119 (10^{-5})	
65.0	0.149 (10^{-5})	0.125 (10^{-6})	0.715 (10^{-6})	0.891 (10^{-6})	0.509 (10^{-6})	
75.0	0.966 (10^{-6})	0.575 (10^{-6})	0.496 (10^{-6})	0.466 (10^{-6})	0.282 (10^{-6})	
85.0	0.650 (10^{-6})	0.480 (10^{-6})	0.309 (10^{-6})	0.507 (10^{-6})	0.200 (10^{-6})	
95.0	0.980 (10^{-6})	0.302 (10^{-6})	0.167 (10^{-6})	0.114 (10^{-6})	0.140 (10^{-6})	

81 cm

	Radial Distance From Source (cm)					
	7.810	8.810	13.810	18.810	23.810	28.810
$^{-3}$)	0.998 (10^{-4})	0.516 (10^{-4})	0.222 (10^{-4})	0.108 (10^{-4})	0.635 (10^{-5})	0.367 (10^{-5})
$^{-4}$)	0.355 (10^{-4})	0.234 (10^{-4})	0.121 (10^{-4})	0.690 (10^{-5})	0.425 (10^{-5})	0.270 (10^{-5})
$^{-4}$)	0.127 (10^{-4})	0.121 (10^{-4})	0.592 (10^{-5})	0.405 (10^{-5})	0.262 (10^{-5})	0.171 (10^{-5})
$^{-5}$)	0.609 (10^{-5})	0.447 (10^{-5})	0.302 (10^{-5})	0.210 (10^{-5})	0.158 (10^{-5})	0.103 (10^{-6})
$^{-5}$)	0.305 (10^{-5})	0.228 (10^{-5})	0.152 (10^{-5})	0.116 (10^{-6})	0.794 (10^{-6})	0.549 (10^{-6})
$^{-5}$)	0.176 (10^{-5})	0.125 (10^{-5})	0.837 (10^{-6})	0.654 (10^{-6})	0.438 (10^{-6})	0.320 (10^{-6})
$^{-5}$)	0.119 (10^{-5})	0.772 (10^{-6})	0.479 (10^{-6})	0.338 (10^{-6})	0.263 (10^{-6})	0.155 (10^{-6})
$^{-6}$)	0.509 (10^{-6})	0.419 (10^{-6})	0.233 (10^{-6})	0.174 (10^{-6})	0.142 (10^{-6})	0.890 (10^{-7})
$^{-6}$)	0.282 (10^{-6})	0.240 (10^{-6})	0.137 (10^{-6})	0.896 (10^{-7})	0.675 (10^{-7})	0.602 (10^{-7})
$^{-6}$)	0.200 (10^{-6})	0.119 (10^{-6})	0.775 (10^{-7})	0.478 (10^{-7})	0.320 (10^{-7})	0.230 (10^{-7})
$^{-6}$)	0.140 (10^{-6})	0.152 (10^{-6})	0.534 (10^{-7})	0.438 (10^{-7})	0.182 (10^{-7})	0.120 (10^{-7})

Table 7. Energy absorption rate (Mev/cm^3-sec) Run 10-22-63, R = 10.00 cm

Horiz. Dist. From Source (cm)	Radial Distance From Sour (cm)					
	10.00	11.00	12.000	13.000	14.000	15
0.0	0.651 (10^{-4})	0.536 (10^{-4})	0.426 (10^{-4})	0.400 (10^{-4})	0.325 (10^{-4})	0.21
5.0	0.359 (10^{-4})	0.322 (10^{-4})	0.296 (10^{-4})	0.246 (10^{-4})	0.213 (10^{-4})	0.14
15.0	0.170 (10^{-4})	0.146 (10^{-4})	0.125 (10^{-4})	0.122 (10^{-4})	0.108 (10^{-4})	0.73
25.0	0.915 (10^{-5})	0.820 (10^{-5})	0.719 (10^{-5})	0.621 (10^{-5})	0.606 (10^{-5})	0.45
35.0	0.640 (10^{-5})	0.517 (10^{-5})	0.442 (10^{-5})	0.391 (10^{-5})	0.362 (10^{-5})	0.26
45.0	0.406 (10^{-5})	0.351 (10^{-5})	0.263 (10^{-5})	0.248 (10^{-5})	0.228 (10^{-5})	0.17
55.0	0.315 (10^{-5})	0.216 (10^{-5})	0.209 (10^{-5})	0.165 (10^{-5})	0.144 (10^{-5})	0.10
65.0	0.193 (10^{-5})	0.163 (10^{-5})	0.142 (10^{-5})	0.108 (10^{-5})	0.984 (10^{-6})	0.67
75.0	0.158 (10^{-5})	0.123 (10^{-5})	0.924 (10^{-6})	0.893 (10^{-6})	0.559 (10^{-6})	0.38
85.0	0.105 (10^{-5})	0.814 (10^{-6})	0.631 (10^{-6})	0.470 (10^{-6})	0.414 (10^{-6})	0.26
95.0	0.104 (10^{-5})	0.678 (10^{-6})	0.435 (10^{-6})	0.308 (10^{-6})	0.338 (10^{-6})	0.19

2-63, R = 10.00 cm

Radial Distance From Source (cm)						
13.000	14.000	15.000	20.000	25.000	30.000	35.000
$0.400\ (10^{-4})$	$0.325\ (10^{-4})$	$0.215\ (10^{-4})$	$0.111\ (10^{-4})$	$0.638\ (10^{-5})$	$0.367\ (10^{-5})$	$0.257\ (10^{-5})$
$0.246\ (10^{-4})$	$0.213\ (10^{-4})$	$0.144\ (10^{-4})$	$0.802\ (10^{-5})$	$0.485\ (10^{-5})$	$0.304\ (10^{-5})$	$0.183\ (10^{-5})$
$0.122\ (10^{-4})$	$0.108\ (10^{-4})$	$0.731\ (10^{-5})$	$0.535\ (10^{-5})$	$0.324\ (10^{-5})$	$0.232\ (10^{-5})$	$0.145\ (10^{-5})$
$0.621\ (10^{-5})$	$0.606\ (10^{-5})$	$0.455\ (10^{-5})$	$0.296\ (10^{-5})$	$0.219\ (10^{-5})$	$0.148\ (10^{-5})$	$0.970\ (10^{-6})$
$0.391\ (10^{-5})$	$0.362\ (10^{-5})$	$0.263\ (10^{-5})$	$0.172\ (10^{-5})$	$0.122\ (10^{-5})$	$0.917\ (10^{-6})$	$0.654\ (10^{-6})$
$0.248\ (10^{-5})$	$0.228\ (10^{-5})$	$0.172\ (10^{-5})$	$0.918\ (10^{-6})$	$0.718\ (10^{-6})$	$0.534\ (10^{-6})$	$0.354\ (10^{-6})$
$0.165\ (10^{-5})$	$0.144\ (10^{-5})$	$0.103\ (10^{-5})$	$0.576\ (10^{-6})$	$0.476\ (10^{-6})$	$0.295\ (10^{-6})$	$0.214\ (10^{-6})$
$0.108\ (10^{-5})$	$0.984\ (10^{-6})$	$0.674\ (10^{-6})$	$0.351\ (10^{-6})$	$0.307\ (10^{-6})$	$0.179\ (10^{-6})$	$0.140\ (10^{-6})$
$0.893\ (10^{-6})$	$0.559\ (10^{-6})$	$0.381\ (10^{-6})$	$0.231\ (10^{-6})$	$0.159\ (10^{-6})$	$0.101\ (10^{-6})$	$0.982\ (10^{-7})$
$0.470\ (10^{-6})$	$0.414\ (10^{-6})$	$0.269\ (10^{-6})$	$0.151\ (10^{-6})$	$0.999\ (10^{-7})$	$0.742\ (10^{-7})$	$0.537\ (10^{-7})$
$0.308\ (10^{-6})$	$0.338\ (10^{-6})$	$0.191\ (10^{-6})$	$0.116\ (10^{-6})$	$0.540\ (10^{-7})$	$0.413\ (10^{-7})$	$0.384\ (10^{-7})$